DAA/Marshall

DIAGNOSIS OF VERTICAL MOTIONS FROM VAS RETRIEVALS DURING A CONVECTIVE OUTBREAK

Final Report
Contract NAS8-35330

by

Theodore W. Funk
Henry E. Fuelberg

Department of Earth and Atmospheric Sciences
Saint Louis University
Saint Louis, Missouri 63103

Prepared for

George C. Marshall Space Flight Center
National Aeronautics and Space Administration
Marshall Space Flight Center, AL 35812

August 1985

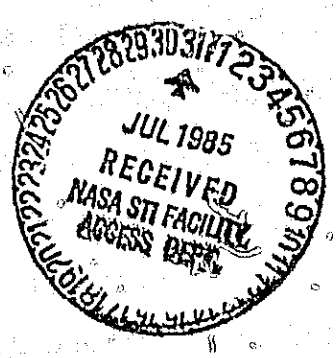

DIAGNOSIS OF VERTICAL MOTIONS FROM VAS RETRIEVALS DURING A CONVECTIVE OUTBREAK

Final Report
Contract NAS8-35330

by

Theodore W. Funk
Henry E. Fuelberg

Department of Earth and Atmospheric Sciences
Saint Louis University
Saint Louis, Missouri 63103

Prepared for

George C. Marshall Space Flight Center
National Aeronautics and Space Administration
Marshall Space Flight Center, AL 35812

August 1985

ABSTRACT

GOES-VAS satellite retrievals are used to investigate an intense convective outbreak over the Mississippi River Valley on 21-22 July 1982. The primary goals are to assess the strengths and weaknesses of three methods for computing vertical motion using satellite retrievals and to determine the effects of short interval observations on the calculations. Then, the vertical motions are incorporated with thermodynamic parameters to assess the usefulness of VAS data in delineating factors leading to storm formation.

Results indicate that the quasi-geostrophic omega equation provided patterns and magnitudes most consistent with observed weather events and the 12 h radiosonde-derived motions. The vorticity method generally produced reasonable patterns, especially over the convective outbreak, although magnitudes were large due to its time derivative. The adiabatic technique gave very poor results because diurnal temperature variations extended from the surface through 600 mb, and there apparently was a compensating effect in the retrieval algorithm that produced opposite fluctuations near 300 mb. These short term variations caused local changes to dominant horizontal advection, producing total motions that did not agree with synoptic conditions even though patterns from advection alone were quite good. Thus, results from time

derivatives were not as encouraging as hoped, especially for 1 h data. Finally, VAS retrievals were of limited use in detecting changes in Lifted Indices because fluctuations could be inferred from routine surface reports. Although patterns of precipitable water were reasonable, time variations were suspect since they could not be confirmed with ground-based data. Nonetheless, in general, VAS retrievals were a useful supplement to the traditional 12 h radiosonde reports.

ACKNOWLEDGEMENTS

The authors thank Drs. James T. Moore and Yeong-jer Lin for their helpful comments and suggestions. Special thanks go to Capt. Michael Remeika (USAF) and Mr. Jonathan Martin for their contributions to the thermodynamic calculations. Also deserving acknowledgement are Ms. Rhonda Webb, who typed the manuscript, and Mr. Kouassi Kouakou, who helped in figure preparation.

The National Aeronautics and Space Administration sponsored this research through Contract NAS8-35300 under the auspices of the Atmospheric Sciences Division, Systems Dynamics Laboratory, Marshall Space Flight Center, AL. Mr. Gary Jedlovec and Mr. David Keller of NASA/Marshall supplied the satellite data and offered many helpful suggestions. Finally, we appreciate the encouragement of Drs. Gregory Wilson (NASA/Marshall) and James Dodge (NASA Hq).

TABLE OF CONTENTS

TABLE OF CONTENTS (CONTINUED)

LIST OF TABLES

LIST OF FIGURES

LIST OF FIGURES (CONTINUED)

LIST OF FIGURES (CONTINUED)

1. Introduction

Synoptic and planetary scales of motion include many atmospheric systems, but numerous other important meteorological phenomena occur on smaller scales. Mesoscale features have typical wavelengths of 1-1000 km and periods of several hours and include systems such as thunderstorms, land/sea breezes, and frontal rainbands. Although our knowledge of, and ability to forecast synoptic scale events has advanced considerably during the past several decades, corresponding improvements at the mesoscale have been much more limited. There are at least two explanations for forecasting limitations in mesometeorology. First, mathematical and theoretical difficulties inhibit the development of prediction models. Second, although large amounts of data are needed to accurately describe these features, only a short time is available for data processing. The current radiosonde network, having a spacing of 400 km and providing data at 12 h intervals, is insufficient for this purpose.

Accurate forecasts of severe convective storms are a major challenge for meteorologists. Due to data limitations, forecasts have been made from a synoptic scale perspective. Soon, however, it is hoped that meteorological satellite technology will make a major impact on severe storm prediction. Specifically, the Visible Infrared Spin-Scan Radiometer (VISSR) Atmospheric Sounder

(VAS), contained on the most recent GOES series, provides radiance data from which mesoscale retrievals of atmospheric temperature and water vapor can be obtained. Complete descriptions of the VAS instrument are given by Menzel *et al.* (1981), Smith *et al.* (1981b), and Chesters *et al.* (1982). Soundings having spatial and temporal separations of about 100 km and 1 h are available, much smaller than that provided by the radiosonde network. With this new capability, it is hoped that forecasters can use VAS soundings to better predict the development and evolution of severe thunderstorms.

There are three necessary ingredients for thunderstorm initiation: instability, moisture, and a triggering mechanism. Concerning stability and moisture content, several recent investigations have favorably assessed VAS's ability to detect mesoscale variations in both time and space (e.g., Smith *et al.*, 1981a; Lee *et al.*, 1983; Smith, 1983; Chesters *et al.*, 1984). To the author's knowledge, however, there have been no published studies to evaluate satellite-derived fields of vertical motion. That is the purpose of the current paper.

2. Methods of computing vertical motion

Vertical motion is an important atmospheric parameter because it controls the distribution of clouds and precipitation, vertically transports mass, moisture, and momentum, and releases the instability of the pre-convective environment. Since magnitudes of vertical motion in the free atmosphere are usually only several centimeters/second for synoptic scale systems, accurate determination is elusive because direct physical measurements are impossible. Instead, indirect techniques, utilizing other atmospheric quantities, must be employed. Miller and Panofsky (1958) cite five schemes for computing large scale vertical motion, i.e., the kinematic, adiabatic, precipitation, vorticity, and numerical (omega equation) methods. All but the precipitation procedure are explored in the current study. Each technique is based on quite different physical and mathematical assumptions and, therefore, possesses different strengths and weaknesses that are described below.

a. Kinematic method

The kinematic procedure is based on the continuity equation in which divergence of the horizontal wind is integrated upward. Vertical motion in isobaric coordinates ($\omega = dp/dt$) is given by

$$\omega_p = \omega_{p+\Delta p} + (\overrightarrow{\nabla \cdot \vec{V}_2})\Delta p \,, \qquad (1)$$

where $\vec{V}_2$ is the horizontal wind and Δp is positive. There are several advantages to the kinematic technique. These include simplicity of calculation, lack of stringent physical assumptions, and the absence of time derivatives. On the other hand, a significant disadvantage is that errors in the measured winds accumulate during the step-wise integration to produce unrealistic ω in the upper troposphere. For this reason, adjustment procedures, such as those by O'Brien (1970) and Peddar (1981), often are used to modify the profiles to a predetermined value (usually zero) at the top most level (usually 100 mb).

b. Adiabatic method

This method is derived from the First Law of Thermodynamics by assuming adiabatic flow. Vertical motion can be computed from

$$\omega = \frac{-\vec{V}_2 \cdot \vec{\nabla}\theta - \partial\theta/\partial t}{\partial\theta/\partial p} , \qquad (2)$$

where θ is potential temperature. A simple mathematical formulation and an insensitivity to wind errors, so that geostrophic values can be used, are important advantages. However, three disadvantages are a time derivative that may be inadequately described by 12 h radiosonde data, inaccurate results when the atmospheric lapse rate approaches the adiabatic value, and an inability to properly represent diabatic motions.

c. Vorticity method

Quasi-geostrophic theory is applicable to large scale systems in which there is a quasi-equilibrium between horizontal forces. The formulation for the vorticity method is obtained from integration of the quasi-geostrophic vorticity equation (Holton, 1979) yielding, in isobaric coordinates

$$\omega_p = \omega_{p+\Delta p} + \frac{1}{f_o}\overline{[-\partial \zeta_g/\partial t - \vec{V}_g \cdot \vec{\nabla}(\zeta_g + f)]}\Delta p \ , \qquad (3)$$

where $\vec{V}_g$ is geostrophic wind, ζ_g is geostrophic vorticity, and f and f_o are variable and constant values of the Coriolis parameter, respectively. Strengths of the method are ease of calculation, use of geostrophic winds, and the ability to neglect complex terms such as tilting, friction, and the vertical advection of vorticity. Weaknesses include possible violation of the underlying assumptions during ageostrophic conditions and, as in the kinematic technique, an accumulation of data errors during step-wise integration. Finally, as noted for the adiabatic technique, the time derivative (of vorticity) may be unrepresentative when 12 h data are employed.

d. Numerical method

The omega equation is derived by eliminating time derivatives in the vorticity and thermodynamic energy equations. The complexity of the result depends on the number of simplifying assumptions, ranging from the general balance equation,

containing twelve forcing functions, to the quasi-geostrophic omega equation, having only the two dominant processes of the complete version. The quasi-geostrophic omega equation is (Holton, 1979)

$$(\nabla^2 + \frac{f_o^2}{\sigma}\frac{\partial^2}{\partial p^2})\omega = \frac{-f_o}{\sigma}\frac{\partial}{\partial p}[-\vec{V}_g \cdot \vec{\nabla}(\zeta_g + f)] - \frac{R}{\sigma p}\nabla^2[-\vec{V}_g \cdot \vec{\nabla}T], \quad (4)$$

where R is the dry air gas constant and σ ($= \frac{-RT\partial\theta}{p\theta\partial p}$), representing stability, varies only in the vertical and with time. The left side of this equation, a kind of three-dimensional Laplacian, can be approximated by ω multiplied by a negative coefficient. The right side contains forcing functions involving the vertical derivative of absolute geostrophic vorticity advection and the Laplacian of geostrophic temperature advection. Thus, upward motion should occur east of height troughs and in areas of maximum warm air advection. A criticism of this formulation is that the two forcing functions usually are not independent because each contains a common component. Therefore, alternative representations have been proposed (e.g., Hoskins et al., 1978; Trenberth, 1978).

Three advantages of the quasi-geostrophic omega equation are its explanation of several empirical rules of synoptic meteorology, relative ease of calculation, and a lack of time derivatives. A disadvantage is the possible violation of quasi-geostrophic theory for subsynoptic scale motions and for strongly baroclinic systems where diabatic processes are important.

e. Past studies

Based on radiosonde data, the kinematic method generally is considered to provide the most reasonable synoptic scale vertical velocities, i.e., those which best correspond to observed map features and cloud/precipitation patterns. The numerical method appears to be the second ranked procedure. Specifically, Smith (1971) found that results from the omega equation were comparable to kinematic values. In a later study, however, the kinematic technique was clearly superior to the omega equation (Vincent et al., 1976). This was confirmed by Smith and Lin (1978) who noted that the kinematic procedure outperformed both the general balance and quasi-geostrophic omega equations. They speculated that the kinematic method was better able to capture smaller scale processes than the numerical approach. In fact, recent studies have shown that mesoscale vertical motions can be successfully calculated using the kinematic technique (Fankhauser, 1969; Moore and Fuelberg, 1981; Fuelberg and Printy, 1983).

Comparisons between different forms of the numerical method have produced contrasting conclusions. For example, Smith and Lin (1978) noted that the simple omega equation was superior to the general balance equation during intense cyclone development. However, Krishnamurti and Moxim (1971) and Pagnotti and Bosart (1984) emphasized that latent heat release could be an important forcing function for vertical motion in some situations. Moreover, Haltiner et al. (1963) demonstrated that frictional

effects markedly influenced ω fields in the lower troposphere.

The adiabatic method generally has been a less reliable indicator of large scale vertical motion than the kinematic and numerical techniques (e.g., Hansen and Thompson, 1965; Wilson, 1976). When applied to mesoscale data, adiabatic motions agreed favorably with weather patterns in the lower troposphere; however, they were inferior to kinematic results in the middle troposphere (Fuelberg and Lee, 1982). Concerning the quasi-geostrophic vorticity method, Eliassen and Hubert (1953) and Collins and Kuhn (1954) observed satisfactory agreement between areas of ascent and large scale patterns of precipitation; however, its use has been relatively infrequent.

For radiosonde data, the references cited above suggest that each method can produce reasonable estimates of synoptic scale vertical motion, with best results from the kinematic and numerical procedures. The current objective is to assess the various techniques using VAS satellite retrievals as input. Such an evaluation is appropriate because satellite and radiosonde data are fundamentally different in nature. For example, the radiosonde is virtually a point source sensor, while the satellite's radiometer provides volume-averaged measurements, thereby achieving smoother definitions of atmospheric structure, especially in the vertical. In addition, the satellite's shorter time interval between observations and lack of directly observed winds are important differences. Specifically, the current

investigation will calculate vertical motions at high temporal resolution from the vorticity, adiabatic, and omega equation methods and will assess the strengths and weaknesses of each technique. The kinematic procedure cannot be utilized with VAS retrievals since only geostrophic or gradient winds can be computed thermally. The study also will investigate the common assumption that a shorter time interval would result in more representative vertical velocities in those methods containing a time derivative. Moreover, the ability of each technique to bridge the "gap" between 12 h radiosonde data will be described. The final goal is to incorporate the vertical motions together with satellite-derived fields of water vapor content and stability to diagnose causes for an intense convective outbreak over the middle Mississippi River Valley.

3. Methodology

a. VAS retrieval procedures

The period 21-22 July 1982 was chosen for study because it contained significant afternoon convection during a period when VAS satellite data were available. It is a typical case in that the entire data region was not cloud-free before thunderstorm development. Six sounding times were available: 1100, 1300, 1600, 1700, 2000, and 2300 GMT 21 July. Separate northern and southern image sectors of the domain were collected, but, due to the small time difference between them (about 30 min), they were treated as a single image for retrieval purposes. This consolidation may be a slight source of error in the 1 h (1600-1700 GMT) changes of temperature, vorticity and thermodynamic parameters that follow. The 1300 and 1600 GMT image pairs were made during the satellite's Dwell Image (DI) mode of operation, while the remaining data were obtained during the Dwell Sounding (DS) mode. The DS mode generally is expected to give somewhat better retrievals of temperature and moisture because of its larger spin budget. Smith et al. (1981b) give a complete description of these modes.

VAS retrievals were prepared at the NASA/Marshall Space Flight Center using techniques incorporating the Man-computer

Interactive Data Access System (McIDAS) (Smith et al., 1979). The physical retrieval algorithm of Smith (1983) was employed; the procedure adds details of temperature and moisture to a "first guess" profile. For the initial sounding time (1100 GMT 21 July), the first guess was from a National Meteorological Center (NMC) 12 h forecast valid at 1200 GMT 21 July. After 1100 GMT, VAS retrievals from the previous times were used as first guesses. The output soundings then were edited via McIDAS with inconsistent data being deleted.

The VAS retrievals underwent a second round of editing at Saint Louis University. The objectives were to locate any remaining anomalous features before objective analysis, obtain a working knowledge of the data, and estimate the smallest wavelength at which VAS data provided meaningful information. To achieve these goals, constant pressure analyses of several basic and derived parameters were prepared. Results were checked closely for vertical stacking, time continuity, appropriateness of gradients, and cloud contamination. Deletions were made as necessary. Finally, sounding data were created at 100 mb intervals from the mandatory levels originally supplied. Standard temperature interpolation and hypsometric procedures were used.

b. Objective analysis of VAS retrievals

Since the convective outbreak occurred over the central one-third of the United States, this was the area of focus.

Locations of edited soundings within the region are shown in Fig. 1. In selecting the grid interval and response characteristics for the objective analysis, the procedures of Koch et al. (1983) were considered. Table 1 gives the number of soundings (after editing) within the analysis region at each time. Retrievals have an average spacing of 110 km in relatively clear areas, but due to cloud cover over certain regions, the separation is not uniform (Fig. 1). Therefore, the "random data spacing", the average separation for a uniform sounding distribution, was calculated (Koch et al., 1983). Since the random spacing (Table 1) was always greater than that in clear areas alone (110 km), especially at 1100 GMT, clustering is indicated. Because of its limited and highly clustered data, 1100 GMT was not utilized for later calculations.

Due to the grouping of the data and ambiguity as to the smallest scale that VAS soundings are meaningful, meso β-scale resolution was not attempted. Instead, for thermodynamic calculations only, the retrievals were treated as a meso α-scale data source, assuming an average spacing of 250 km. The Barnes (1973) objective analysis procedure was employed on a grid mesh of 127 km. Response parameters that retained 62% of amplitudes at wavelengths of 500 km (twice the assumed VAS spacing), i.e., 89% at 800 km (twice the radiosonde spacing), were utilized. Fig. 2 shows that the objective analysis for geopotential height at 500 mb for 1600 GMT (middle) has removed most meso β-scale features

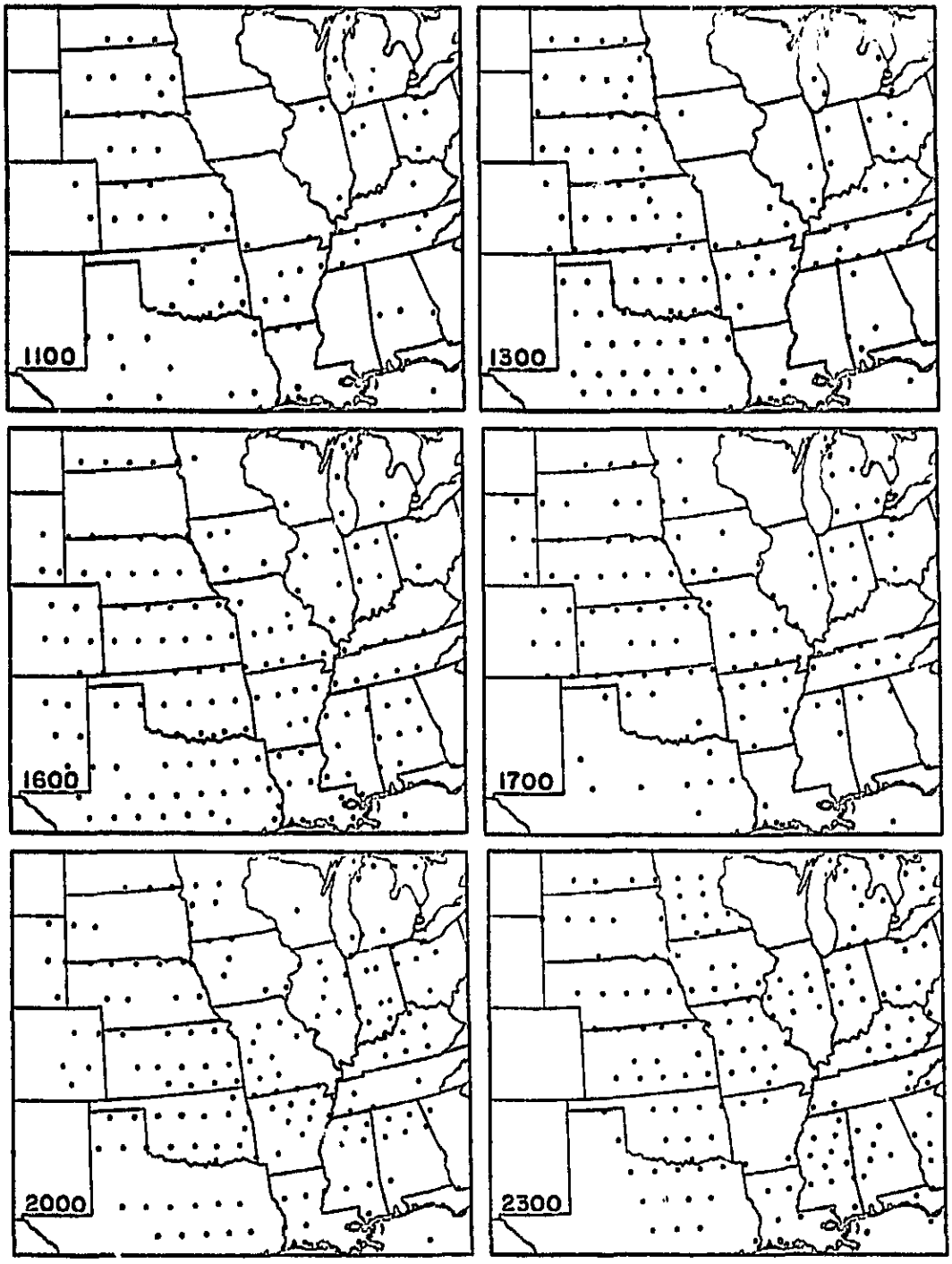

Fig. 1. Locations of edited VAS retrievals at the six observation times.

Table 1. Number of soundings after editing within the computational domain. Their separation, if uniformly distributed, is also shown.

Scunding Time (GMT)	Number of soundings	Random data spacing (km)
1100	81	245.9
1300	127	191.6
1600	155	171.8
1700	120	197.6
2000	157	170.6
2300	170	163.4

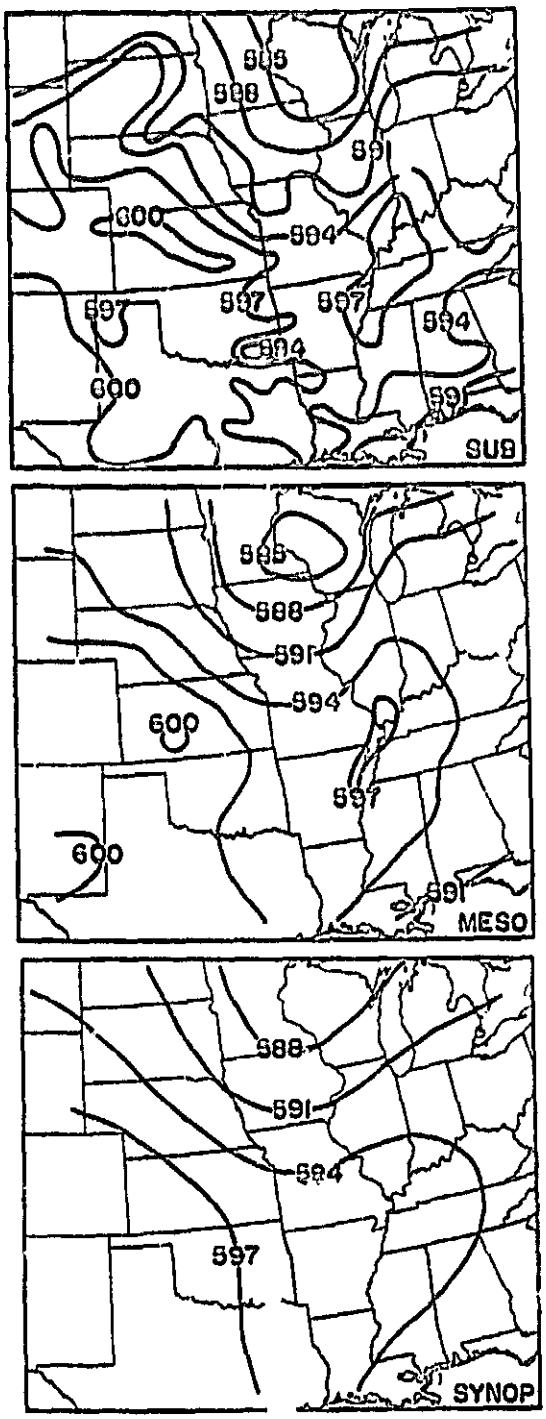

Fig. 2. Subjective and objective analyses of VAS-derived heights at 500 mb for 1600 GMT 21 July 1982. The top panel is the subjective (hand) analysis (SUB) while the middle and bottom sections are meso α (MESO) and synoptic (SYNOP) scale objective versions. Heights are in decameters.

present in the original subjective (hand) analysis (top). Some of these details may have been meteorological phenomena while others were due to data uncertainty, but since most exhibited poor continuity, they were not retained.

While meso α-scale resolution was appropriate for calculating thermodynamic parameters, it was not suitable for preparing vertical motions since several methods employed quasi-geostrophic theory. To obtain the necessary larger scale fields, smoothing of the meso α-scale grids was considered, e.g., Shuman ('957): however, it was decided to begin the analysis process anew, this time with synoptic scale response parameters that retained only 3% of amplitudes at 500 km wavelengths (i.e., 27% at 800 km). Thus, heights using the new response (bottom of Fig. 2) are considerably smoother than those at the finer resolution. Specifically, meso α-scale features are greatly filtered while larger scale wavelengths are retained. To verify the suitability of the analyzed data for quasi-geostrophic calculations, Rossby numbers (R_o) were computed using $R_o = |\vec{V}_2|/fL$, where L, the scale length, is one-fourth of the actual wavelength. Results of approximately 0.1 verified the large scale character of the fields.

a. Radiosonde data

Radiosonde data were obtained from the National Climatic Center. Although four times were investigated, i.e., 0000 and 1200 GMT on 21-22 July 1982, the two middle observations were

most important since they served as bracketing times for the VAS retrievals. Data at 100 mb intervals were prepared using the previously mentioned procedures. The Barnes (1973) technique again was employed to grid the data, but in this case a 60% response at 800 km separation (two times the average station spacing) was utilized for thermodynamic calculations. As with the VAS data, the grid interval was 127 km. For consistency with the satellite-derived vertical motions, corresponding values from radiosonde data were calculated from grids again having a 27% response at 800 km separation. In addition, due to the availability of observed winds, vertical motions also were calculated using the kinematic procedure.

4. Weather conditions

As is typical of summer, 21-22 July was not an especially baroclinic situation, although there was significant convective activity. One tornado, two cases of large hail, and fifteen occurrences of damaging winds were documented within the grid network during the 24 h period beginning at 1200 GMT 21 July. Additional severe weather occurred afterwards. Fig. 3 shows National Meteorological Center (NMC) analyses for 0000 GMT 21 July through 1200 GMT 22 July. It should be noted that the period contained active shortwave development, not simply advection of pre-existing features.

At 0000 GMT 21 July, a frontal system extended from the East Coast into Kansas. The western half contained only weak gradients of temperature and dewpoint; however, radar (not shown) revealed scattered thunderstorms over eastern Missouri. A cold front curving from North Dakota to Montana was the system of concern for the middle Mississippi River Valley. At 500 mb, ridging extended from Colorado into the Ohio River Valley. To the north, a developing shortwave had not yet produced appreciable cyclonic flow. No well defined jet streaks were evident at any level (not shown), although strongest winds and the thermal trough were upwind of the wave axis, thereby suggesting further cyclonic development.

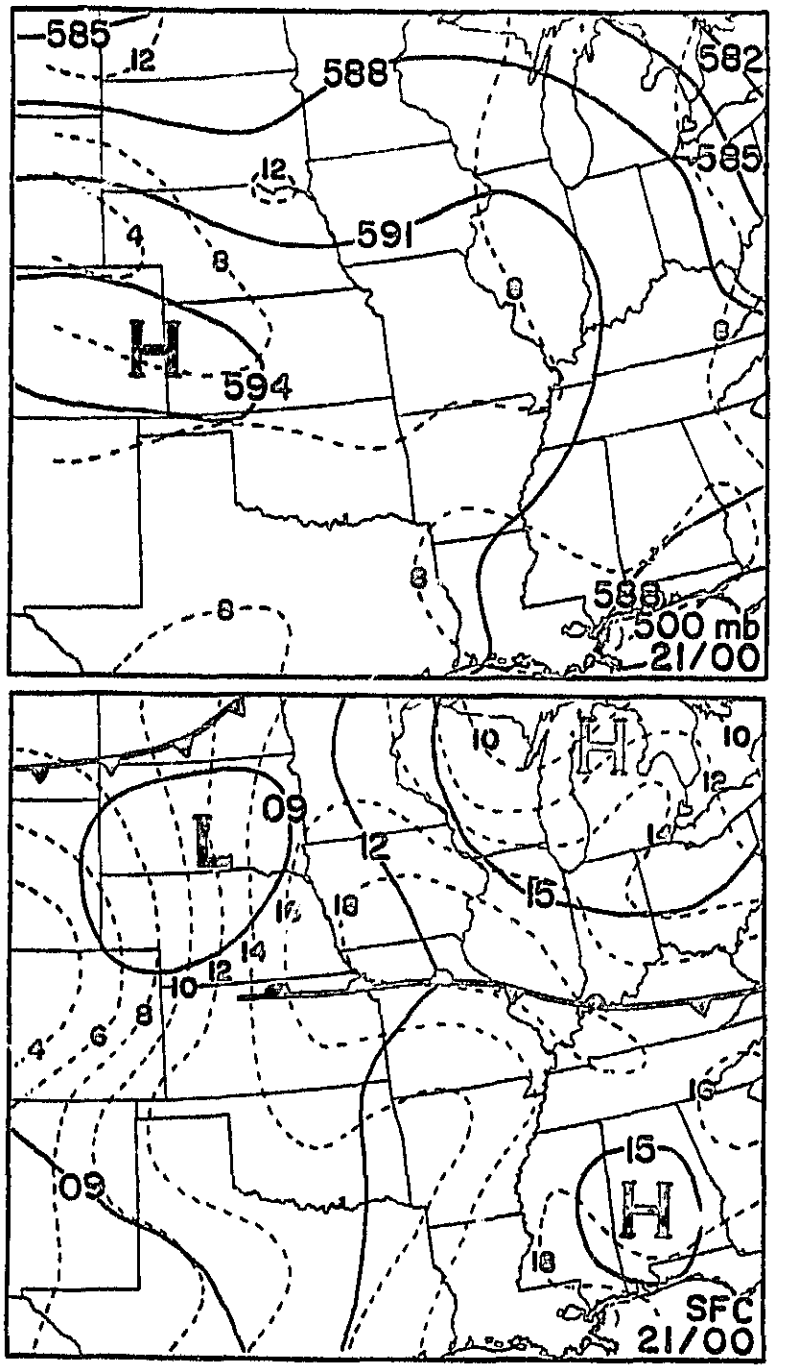

Fig. 3. NMC analyses for the surface and 500 mb between 0000 GMT 21 July and 1200 GMT 22 July. At the surface, solid lines are isobars at 3 mb intervals while dashed lines depict mixing ratios at intervals of 2 g kg^{-1}. At 500 mb, heights (solid lines) are in decameters while dashed lines denote absolute vorticity (10^{-5} s^{-1}).

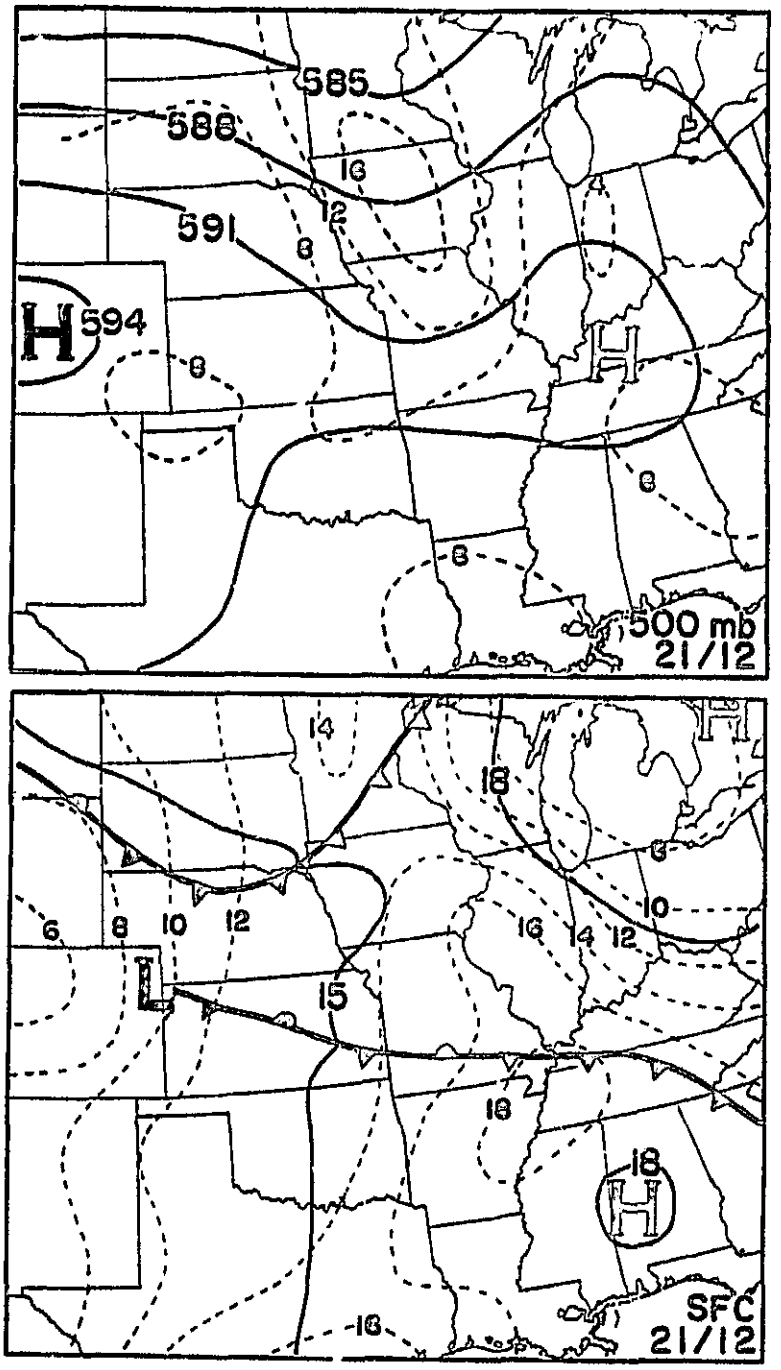

Fig. 3. (Continued)

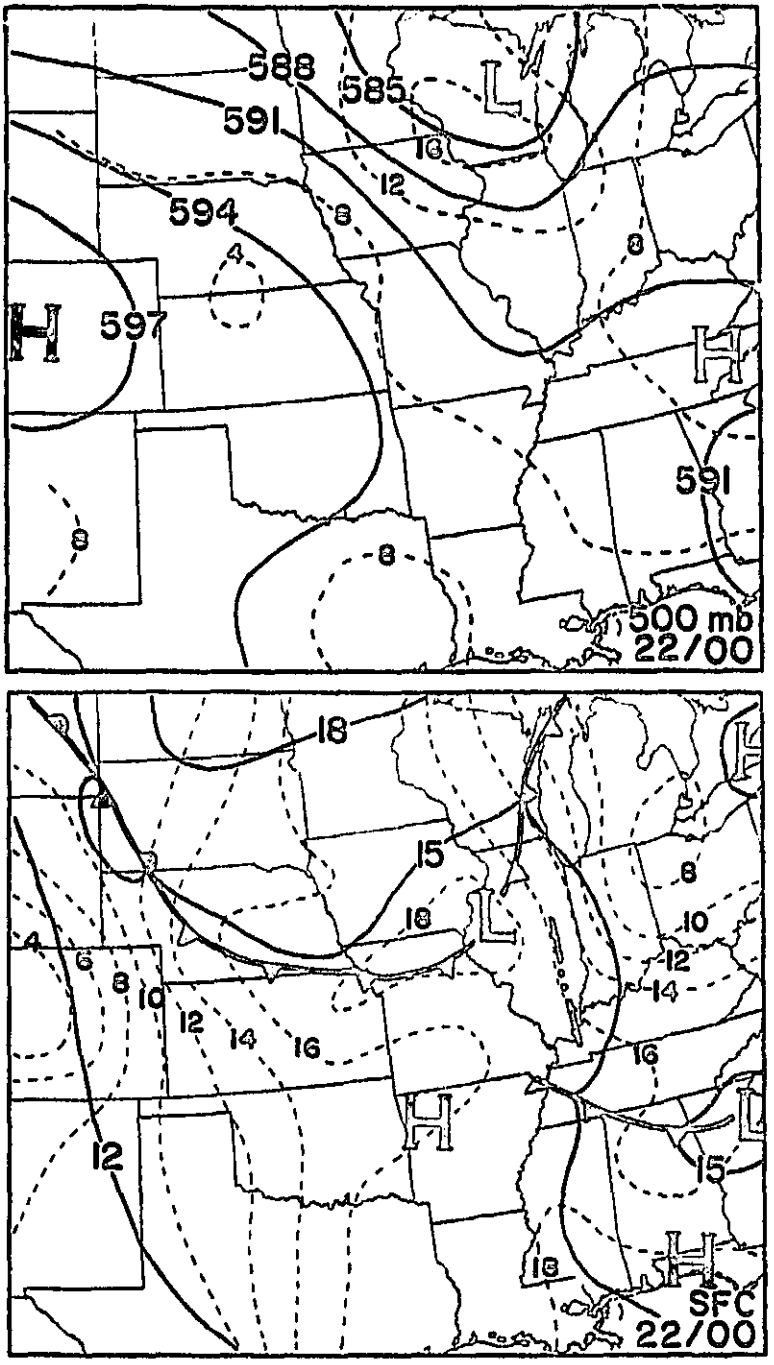

Fig. 3. (Continued)

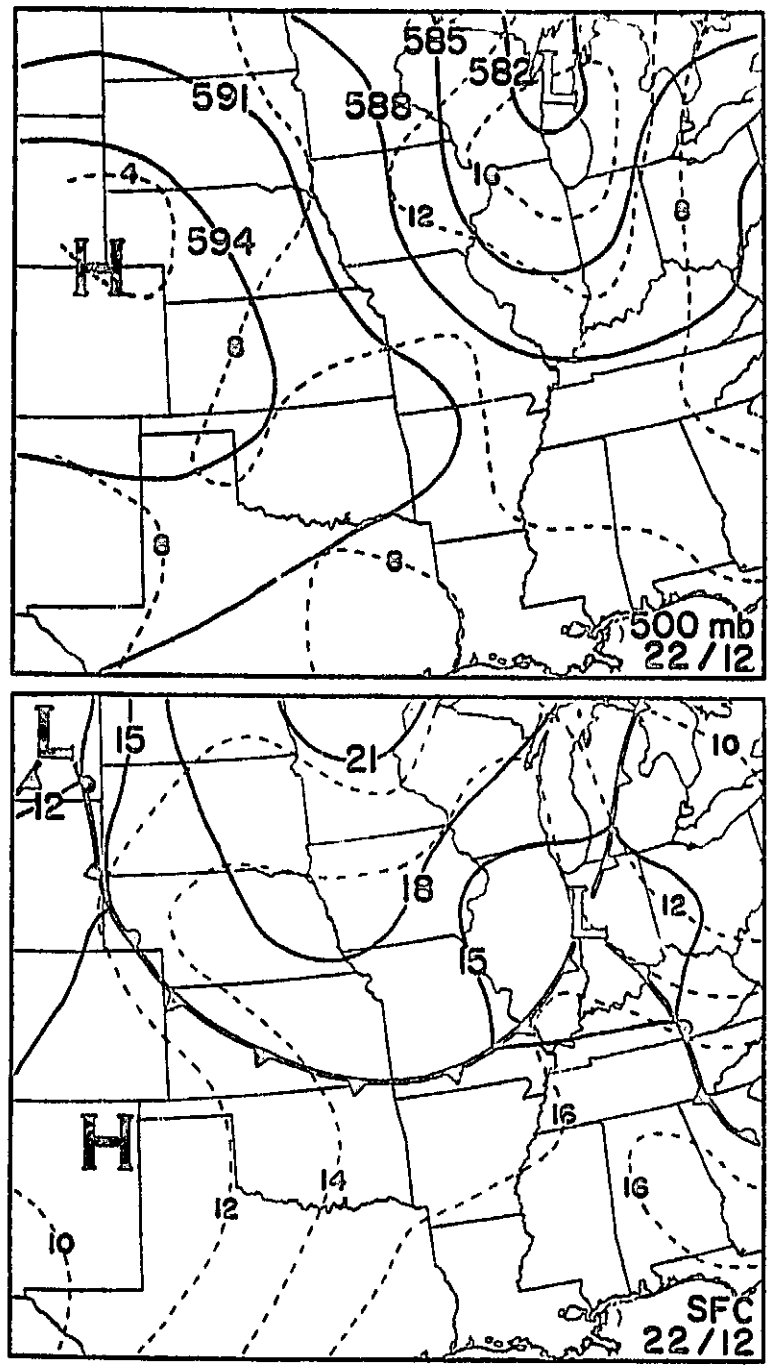

Fig. 3. (Continued)

By 1200 GMT 21 July, the weak front from Missouri to Colorado had become stationary, but the cold front over the Dakotas had progressed southeastward, now extending from Wisconsin to Nebraska. Thunderstorm activity was associated with this front (not shown); however, the convection over eastern Missouri had virtually dissipated. At 500 mb, the shortwave had amplified, causing the ridge over the South to become "pinched off" with a second high over Kentucky. This ridge suppressed convective activity in the pre-storm environment. A vorticity maximum was positioned over central Iowa with positive vorticity advection (PVA) inferred through Illinois. Maximum winds (not shown) continued on the upwind side of the trough, and a jet streak (25-30 m s^{-1}) had developed at 200 mb.

Renewed storm activity over the middle Mississippi River Valley, the emphasis of the current study, began near 1735 GMT. This was a preferred area for convective development. At the surface (Fig. 3), an axis of high mixing ratios (>16 g kg^{-1}) extended from the Gulf Coast through western Illinois (equivalent to dewpoints of about 21-23°C), while at 850 mb (not shown), values of 15-16 g kg^{-1} were evident over western Illinois. In addition, temperatures greater than 34°C (not shown) stretched from central Arkansas into southern Illinois at midday. Thus, the region was quite unstable with 1200 GMT Lifted Indices (LI) ranging from -2 to -5. Given the instability and adequate water vapor, only a triggering mechanism was needed to initiate convec-

tion.

Hourly satellite imagery beginning at 1600 GMT (Fig. 4) reveals thunderstorm development in several locations. Although large scale ascent east of the trough is probable over each area, smaller scale forcing appears to be superimposed as well. The first area, having tops to 18.9 km and extending from southeastern Illinois to northern Alabama, likely was associated with the nearby gradient of temperature and mixing ratio (Fig. 3). Although not analyzed by NMC, this appears to be a warm frontal zone. The second and third storm areas, with tops to 16.8 km, were located over Arkansas and southeastern Missouri. Based on hourly GOES imagery as well as surface reports, both appear to have been induced by separate thunderstorm outflow boundaries from earlier convection over western Missouri. In addition, surface streamline analyses (not shown) revealed convergence in these areas. A fourth region of convection developed rapidly over southwestern Illinois, just east of St. Louis, as a cloud mass progressing across Missouri (Fig. 4) moved into a more favorable environment that included abundant moisture and large scale ascent from the middle tropospheric trough and the advancing cold front (Fig. 3). The National Weather Service, recognizing these conditions, had issued a severe weather watch for most of Illinois just prior to rapid storm development. Tops of the ensuing convection exceeded 18.2 km. Finally, afternoon heating and weak cyclonic flow contributed to thunderstorms along the

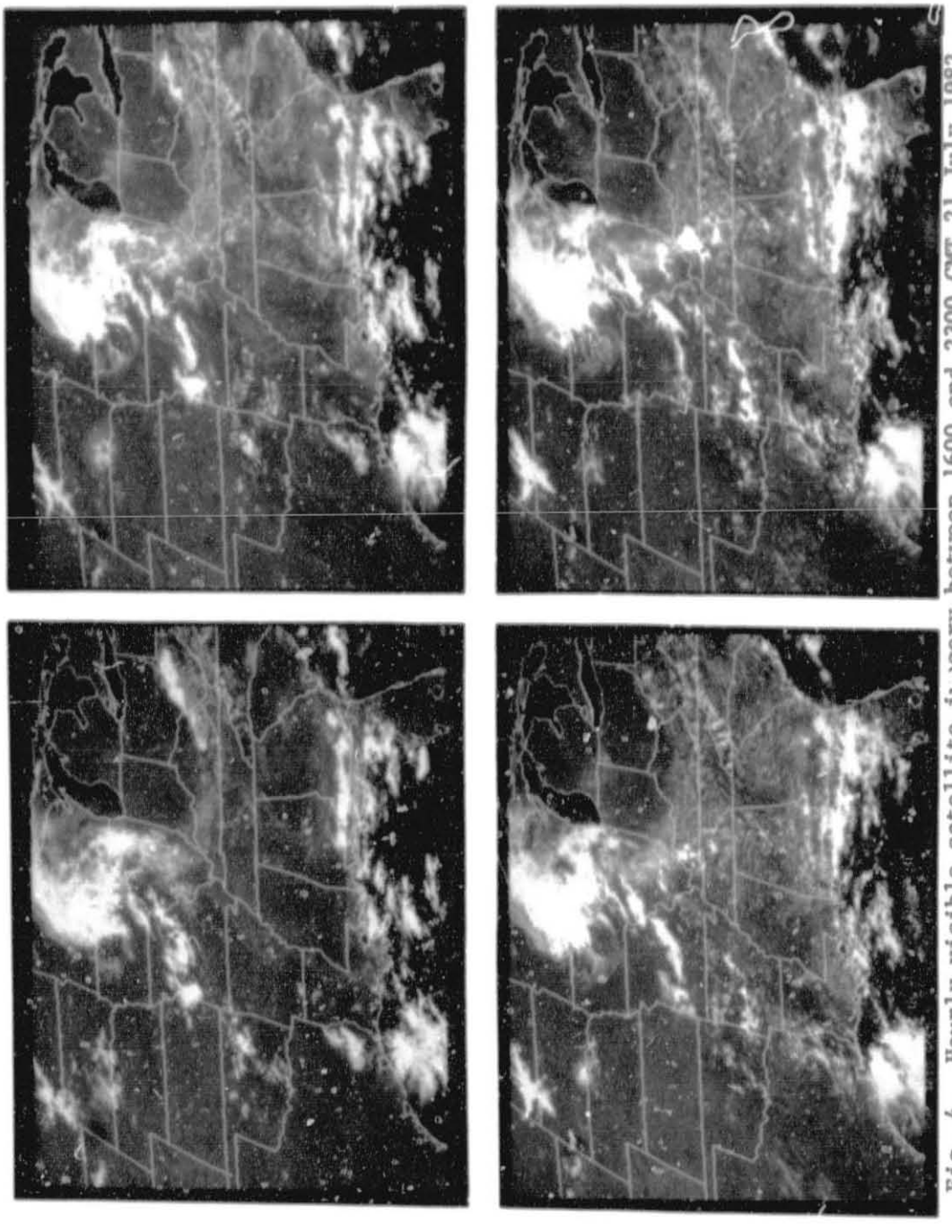

Fig. 4. Hourly visible satellite imagery between 1600 and 2300 GMT 21 July 1982.

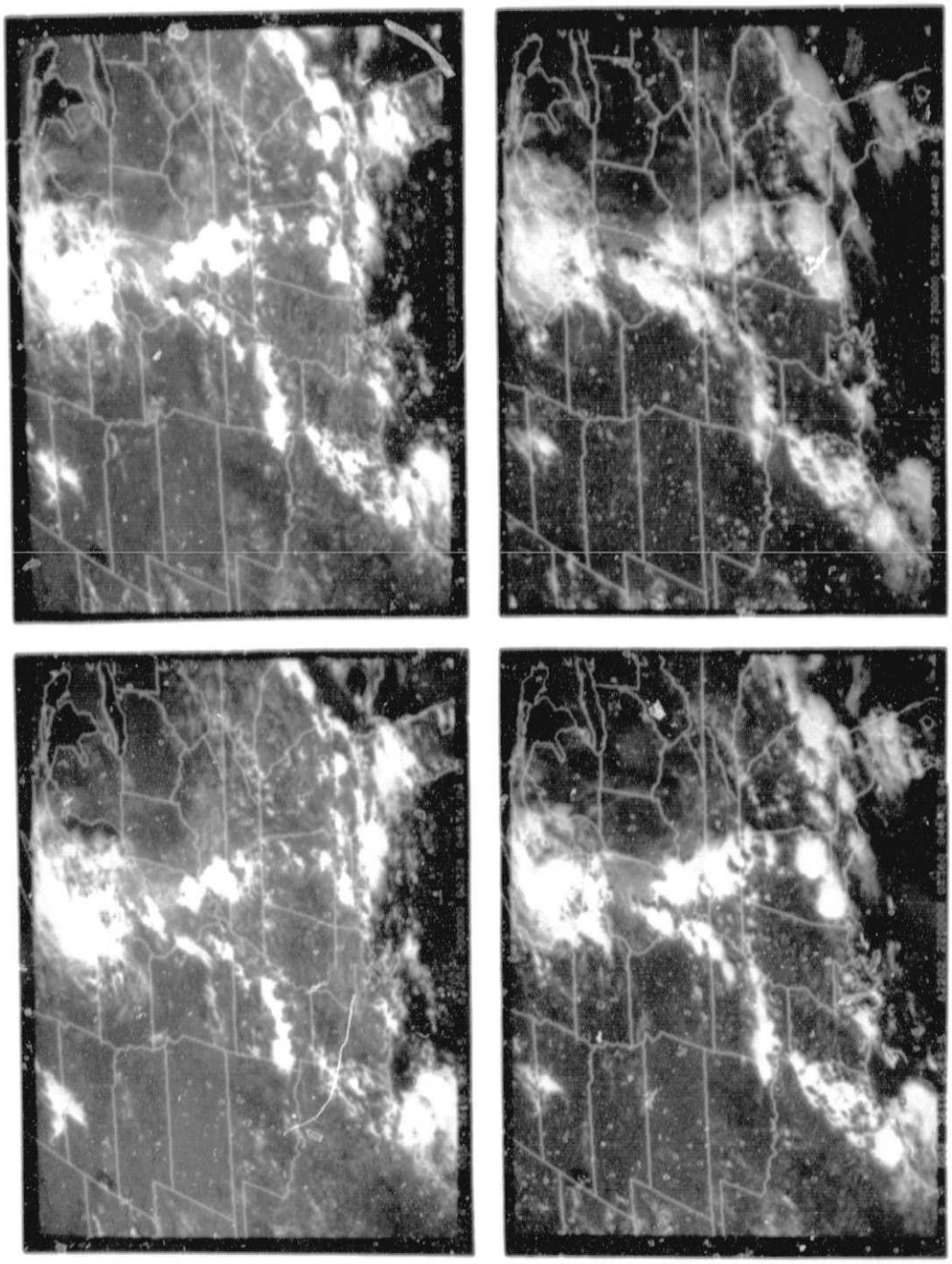

Fig. 4. (Continued)

Gulf Coast States. Of course, the heating likely enhanced instability in the other storm regions as well. For example, satellite imagery (Fig. 4) shows southwest Illinois to be relatively clear before convective development.

By the end of the study period, 0000 GMT 22 July (Fig. 3), the cold front over the southeast had moved little, while the stationary front through Missouri had been omitted by NMC. The cold front over the northwest had continued its advance, and a low had developed along it over Illinois in response to the deepening middle-tropospheric system. Thunderstorms were most intense and widespread near this time with strongest cells (Fig. 4) aligned along the moisture tongue through Illinois and Kentucky (Fig. 3). NMC now carried a squall line in this region. Slight moisture convergence (reaching 0.7 g kg^{-1} h^{-1}) at 850 mb (not shown) was aiding the convection.

At 500 mb, the movement of the deepening shortwave is noteworthy. Specifically, it had advanced into Illinois between 1200 GMT 21 July and 0000 GMT 22 July, thereby triggering thunderstorm development between the two times. The pattern of 500 mb absolute vorticity (Fig. 3) contains a maximum over Wisconsin and a lobe extending southward to Alabama. The lobe is coincident with maximum convective activity. At 200 mb (not shown), the jet streak remained upwind of the trough.

Finally, by 1200 GMT 22 July, twelve hours past the primary study period, the low had moved to western Indiana, sweeping the

cold front through Illinois. NMC now carried a warm front from the low toward the southeast. Although, the majority of thunderstorms had dissipated, some frontal activity continued through Indiana. The strengthening of the surface low was in response to continued shortwave amplification at 500 mb (Fig. 3).

5. Results

This section presents geopotential heights, geostrophic vorticities, and vertical motions calculated from the radiosonde and satellite data. It describes patterns and continuities at the five VAS times, as well as their relationships with the bracketing 12 h radiosonde-derived fields. For heights and vorticities, the 500 mb level will be examined, but for vertical motions, 600 mb is emphasized since it appeared to have the best overall results. Stability and precipitable water are the final parameters discussed.

a. Height and vorticity

Before describing the vertical motions, it is informative to present the more basic parameters of geopotential height and absolute geostrophic vorticity (Fig. 5). Continuity among the five VAS-derived fields is very good at 500 mb in spite of the data gaps noted earlier (Fig. 1). Specifically, the major trough through Iowa and northwest Missouri at 1300 GMT progresses eastward to Wisconsin and Illinois by the last time. The trough amplifies through 1700 GMT but appears to diminish thereafter. Actually, however, heights near the trough continue to fall several meters. The illusion results from strengthening of the eastern high pressure ridge (about 50 m) through 1700 GMT, fol-

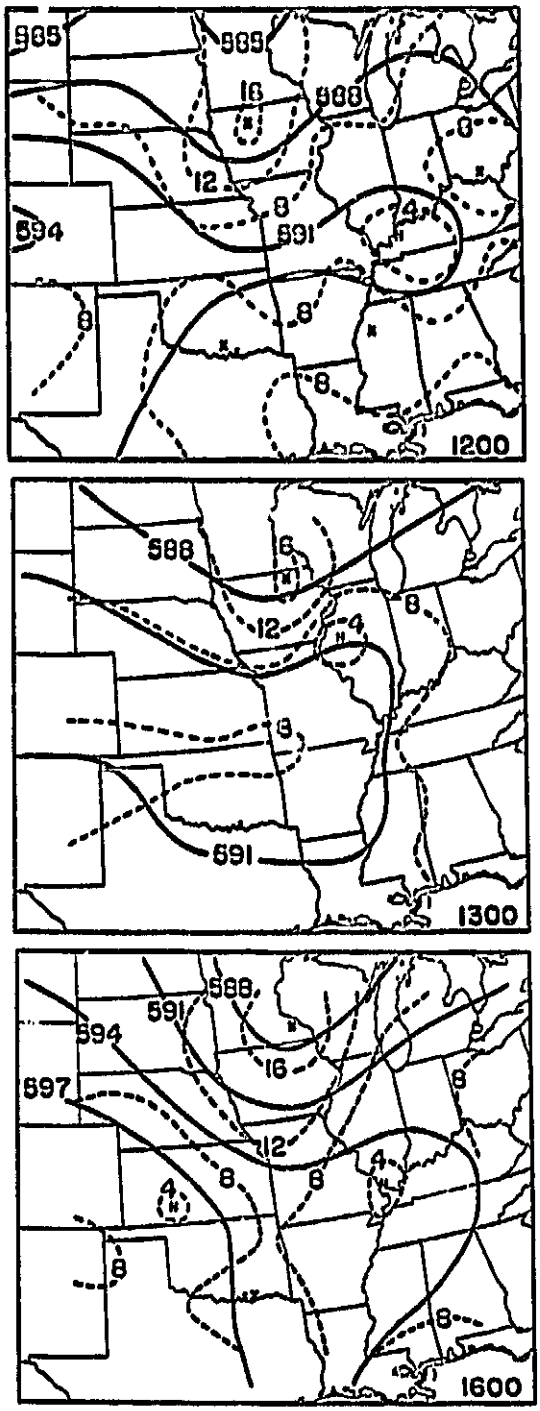

Fig. 5. Heights (solid, in decameters) and absolute geostrophic vorticities (dashed, in 10^{-5} s^{-1}) at 500 mb. Radiosonde-derived analyses are at 1200 GMT 21 July and 0000 GMT 22 July, while the intervening times are from VAS data.

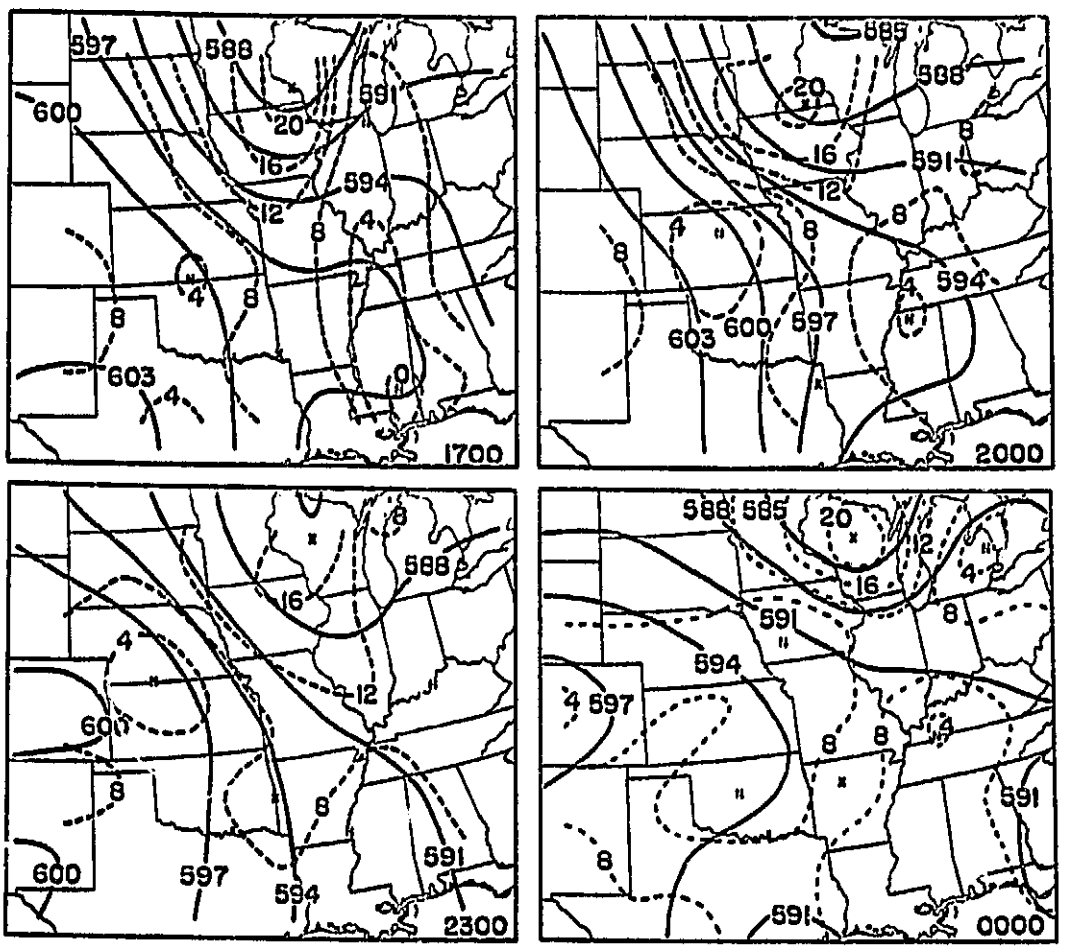

Fig. 5. (Continued)

lowed by weakening. The timing of the shortwave in relation to the storm outbreak is noteworthy. As the trough advances toward Illinois and the inhibiting downstream ridge dissipates and exits, there apparently is ascent that releases the potential instability and initiates the convective outbreak near 1735 GMT (Fig. 4). This will be confirmed in later sections.

Patterns of absolute geostrophic vorticity, computed as the Laplacian of geopotential height, also have very good continuity (Fig. 5). The main vorticity maximum ("X") associated with the shortwave generally propagates slowly northeastward with the trough. Values and gradients are greatest at 1700 GMT, reaching 24×10^{-5} s^{-1} over western Wisconsin. The elongated minimum from the Gulf Coast States through Illinois is well positioned with respect to the height ridge, with smallest values ("N") near the greatest anticyclonic curvature.

A common forecasting tool is to qualitatively assess vertical motion from absolute vorticity advection. Based on the omega equation (4), upward increasing positive vorticity advection (PVA) indicates ascent, whereas upward increasing negative advection (NVA) denotes descent. Also, from the vorticity method (3), Dutton (1976) and others have noted that when strong PVA occurs above approximately 500 mb and/or strong NVA occurs below, there is a contribution to negative ω. Fig. 5 shows that maximum PVA is associated with the northern portion of the shortwave trough and the main cloud area (Fig. 4). Due to orientations of the

height and vorticity isopleths, greatest PVA (6.5×10^{-9} s^{-2}, not shown) and apparent uplift are at 1700 GMT over eastern Iowa and southern Wisconsin. Weak PVA enters western Illinois between 1600-1700 GMT, and is over most of the state by 2000 GMT. This advection is instrumental in the convective development. On the other hand, NVA, and therefore apparent subsidence, are suggested over eastern Kansas and most of Oklahoma, thereby corresponding to the relatively clear skies (Fig. 4).

By comparing patterns from the two data sources (Fig. 5), one can evaluate the satellite's ability to bridge the 12 h gap between conventional soundings. VAS-derived fields at 1300 GMT show good agreement with corresponding radiosonde patterns at 1200 GMT. The main trough and vorticity center move slightly eastward during the 1 h period. In addition, the radiosonde data verify the pre-storm "capping" ridge and vorticity minimum over the middle Mississippi River Valley that is an extension of the main ridge over the Great Plains. Similarly close agreements are found between satellite-derived fields at 2300 GMT and the radiosonde version at 0000 GMT. One again should note the orientation and slight eastward movements of the trough and associated vorticity maximum. Based on the conventional soundings, heights in the trough have fallen 15-20 m since 1200 GMT, but as stated earlier with the VAS data, this is not obvious from the contours alone because of the downstream ridge. The radiosonde soundings also illustrate damping of the ridge over southern Illinois,

thereby verifying results from the VAS retrievals. Finally, progression of the trough axis between the two radiosonde times is depicted well by the intervening VAS observations (Fig. 6). For each successive time, the trough moves further east by an amount proportional to the time interval between observations. The good agreements and continuities noted here confirm the operationally based findings of Anthony and Wade (1983).

Although height patterns from the two data sources agree closely (Fig. 5), a careful inspection shows that values at specific locations sometimes exhibit greater discrepancy. This will affect results from the vorticity method since it contains a time derivative, but with the numerical procedure only patterns at single times are employed. These topics are examined in the following sections.

b. Vorticity method

Fields of vertical motion from the vorticity method are presented for 600 mb in Fig. 7. Radiosonde soundings were utilized at 1200 and 0000 GMT; however, VAS retrievals were input at the other times. For both data sources, backward differencing was employed in the time derivative of geostrophic vorticity ($\partial\zeta_g/\partial t$). An exception was forward differencing at the first VAS time (1300 GMT). Also, for 1700 GMT, instead of utilizing a 1 h time interval, data at 1300 GMT were employed. Reasons for the latter choice are explained later.

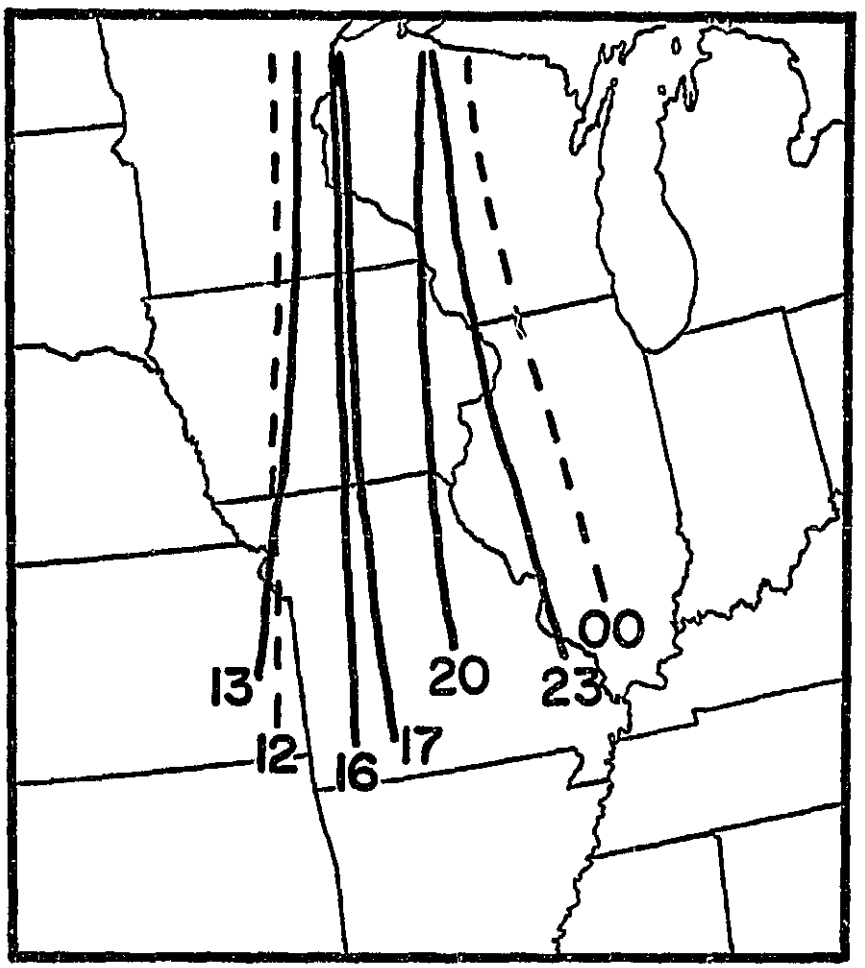

Fig. 6. Approximate locations of trough axes at 500 mb from VAS (solid) and radiosonde data (dashed). 17 denotes 1700 GMT 21 July.

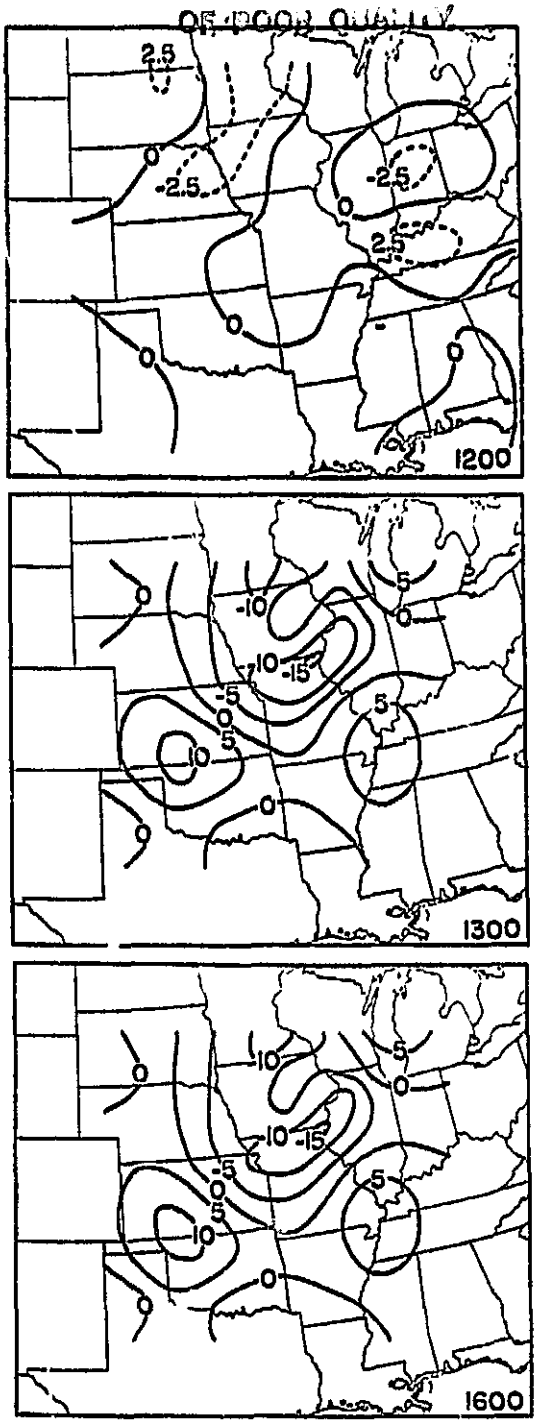

Fig. 7. Vertical motions (μb s^{-1}) at 600 mb from the vorticity method. Radiosonde soundings were utilized at 1200 and 0000 GMT while VAS data were employed at the remaining times. The dashed line at 2000 GMT is the axis for the vertical cross section in Fig. 11. Patterns at 1700 GMT are from a 4 h time derivative using 1300 GMT data.

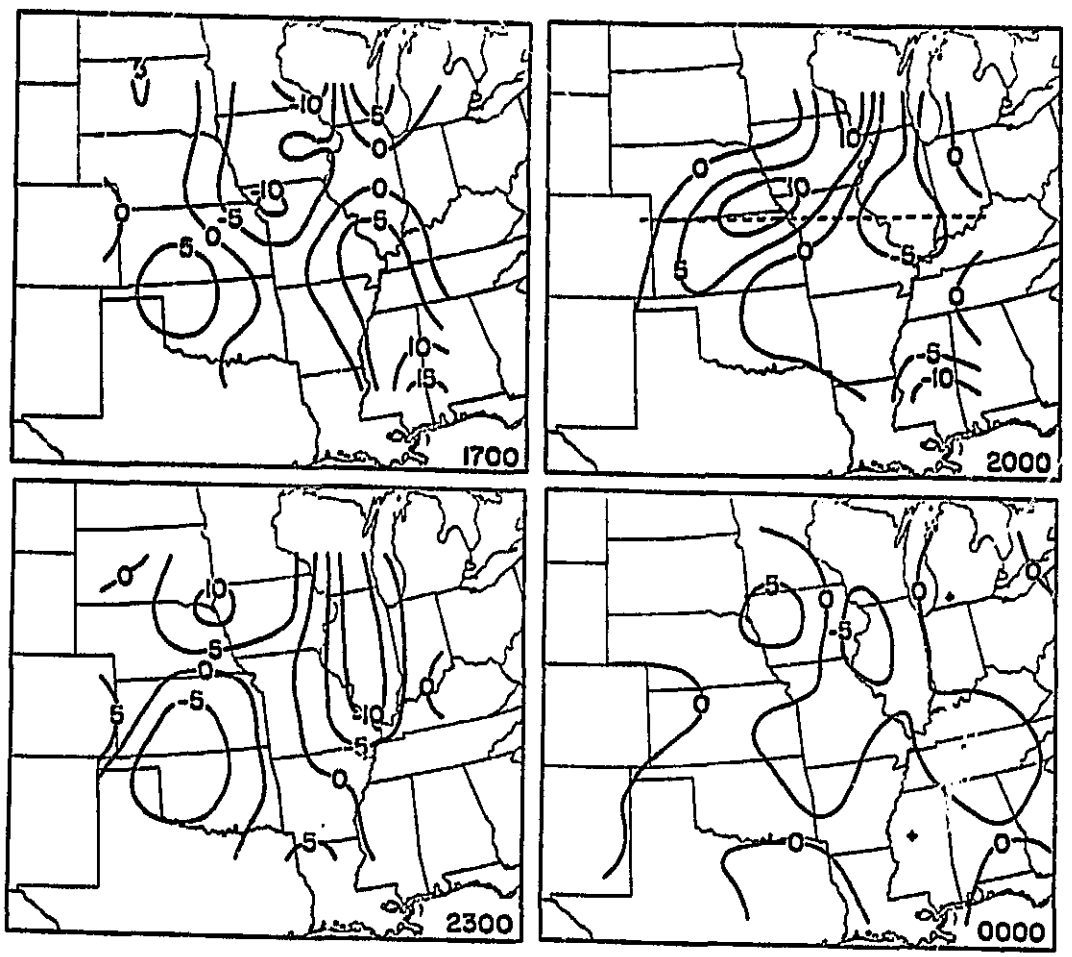

Fig. 7. (Continued)

Continuity between the five VAS times generally is very good. Areas of greatest upward and downward motion correspond closely with the major height and vorticity features (Fig. 5). In this comparison, it is important to note that patterns of height and vorticity at 500 mb are very similar to those at 600 mb (not shown). At 1300 and 1600 GMT, the center of ascent along the Missouri-Illinois border is positioned ahead of the major trough axis. Patterns for these two times appear almost identical because the choices for time differencing produce the same $\partial\zeta_g/\partial t$ component, and it is the dominant contributor to ω. The area of ascent moves little by 1700 GMT, but by 2000 and 2300 GMT, it propagates into Illinois, coincident with the primary storm activity.

Concerning downward motion, a center extends from southern Illinois to western Tennessee through 1700 GMT (Fig. 7), near the ridge and vorticity minimum (Fig. 5). By 2000 GMT, however, it is replaced by the upward motion that initiates the convection. This ability of the vorticity method to delineate vertical motions over the storm area is very encouraging. A second region of positive values is behind the trough over the Northern Plains. It shows reasonable continuity by expanding and moving generally eastward with the shortwave. A final area of descent, initially over Oklahoma and Kansas, is coincident with the ridge and minimum vorticity (Fig. 5). Both areas slowly advance northward by 2000 GMT. However, by 2300 GMT, the signs reverse, with

upward motion now over the Southern Plains. This change is due to positive $\partial\zeta_g/\partial t$, as the area of minimum vorticity moves north to the Kansas-Nebraska border (Fig. 5).

It is informative to document relative contributions of the temporal ($\overline{[-\partial\zeta_g/\partial t]\Delta p}$) and advective ($\overline{[-\vec{V}_g\cdot\vec{\nabla}(\zeta_g + f)]\Delta p}$) components. Fig. 8 shows results at 600 mb integrated from the surface for 2000 GMT. The local derivative (top) is dominant, even though a 3 h interval is utilized. For individual levels (before integration), the time derivative is most influential below 600 mb where advection is weak; however, the components are more comparable in the middle and upper troposphere. Nonetheless, after integration the upper troposphere (not shown) generally is dominated by effects of the local derivative from below. It is interesting to note that the two components oppose one another in the main area of ascent ahead of the trough and in the area of subsidence over northeastern Kansas. This is expected since downwind of troughs, for example, the advection term in (3) produces descent in layers containing PVA, whereas the local increase in vorticity produces ascent. The inverse is true downwind of ridges. Dutton (1976) also noted this tendency for the terms to cancel one another. In current regions of opposition, signs of overall vertical motion usually are determined by the local derivative.

Fig. 9 presents vertical velocities at 1700 GMT based on 1 h time differencing from 1600 GMT data. One should recall that the diagram in Fig. 7 was based on a 4 h interval. In comparing the

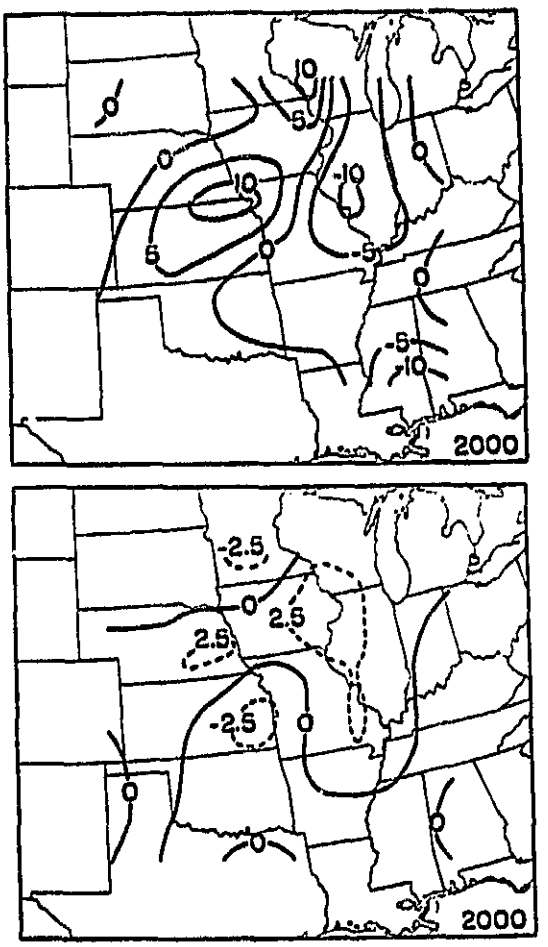

Fig. 8. Temporal ($\overline{[-\partial\zeta_g/\partial t]}\Delta p$, top) and advective ($\overline{[-\vec{V}_g \cdot \vec{\nabla}(\zeta_g + f)]}\Delta p$, bottom) components of vertical motion ($\mu b\ s^{-1}$) from the vorticity method at 600 mb for 2000 GMT.

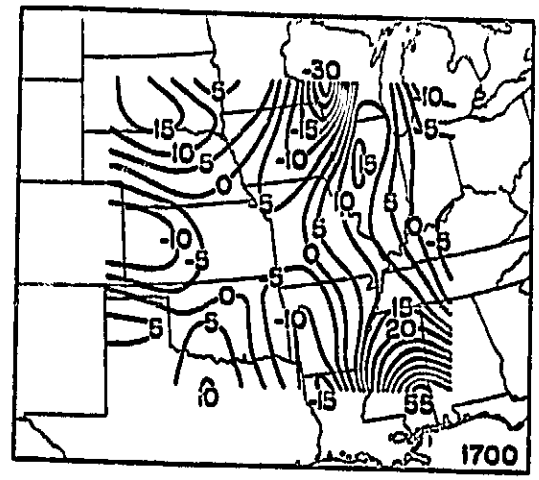

Fig. 9. Vertical motions (μb s^{-1}) from the vorticity method at 600 mb for 1700 GMT; 1 h time differencing from 1600 GMT data was employed.

two diagrams, several similarities are apparent. First, both versions produce ascent near the shortwave trough and over western Arkansas; however, the primary center is displaced further north with the 1 h differencing, causing poor continuity with the other times. Also, the 1 h version contains upward motion over western Kansas that does not occur with the longer time interval. Regions of subsidence from southern Illinois to Mississippi, behind the trough over South Dakota, and over Oklahoma and Texas, are quite similar in each case. However, the center of descent over central Illinois from the 1 h motions does not appear in the 4 h patterns. Concerning magnitudes, motions from the 1 h scheme are approximately triple the 4 h values in the main center of ascent over Wisconsin, and three to four times greater in the areas of descent over Mississippi and North Dakota. Thus, their agreement with the other times (Fig. 7) is poor. At 300 mb (not shown), patterns from both versions are similar, but the 1 h values are unrealistically large, e.g., greatest values are -68 $\mu b\ s^{-1}$ and +130 $\mu b\ s^{-1}$.

Differences in the two versions of 1700 GMT vertical motions are due to the time derivative and can be explained by the vorticity patterns of Fig. 5. Specifically, their continuity is quite good, but magnitudes at particular locations sometimes vary greatly between times. A portion of these fluctuations is due to data uncertainty; however, near the trough, such errors are thought to be a relatively minor component of the overall change.

Effects of data uncertainty can be evaluated by introducing simulated errors into the observed geostrophic vorticities. To maximize the effect, motions due to the $\partial\zeta_g/\partial t$ component were computed at 1700 GMT from perturbed data at 1600 and 1700 GMT. Fig. 10 shows results for the grid point in western Wisconsin that originally had both the largest geostrophic vorticity and upward motion. The top section simulates vorticity errors of +10% (dashed) or -10% (dashed-dot) of the observed algebraic difference at each level. It is obvious that large variations in vertical motion occur for a 1 h interval. Of course, with actual data, errors at individual levels should alternate signs to some extent, thereby providing partial cancellation upon vertical integration. Also, the effects of errors are less if a longer time interval is employed. This clearly is indicated by the bottom section of Fig. 10 which is based on the same perturbations as the top portion, except there is 4 h differencing. These results suggest that 1 h time derivatives are not appropriate for the vorticity method, and that more elaborate procedures may be necessary to take advantage of VAS's 1 h capabilities, at least for those synoptic situations similar to 21 July 1982. For cases with stronger dynamic forcing, the influence of data uncertainty should be smaller; thus, a 1 h time derivative might be more useful.

Having established the continuity of patterns among the five VAS times, their agreement with radiosonde-derived fields now is

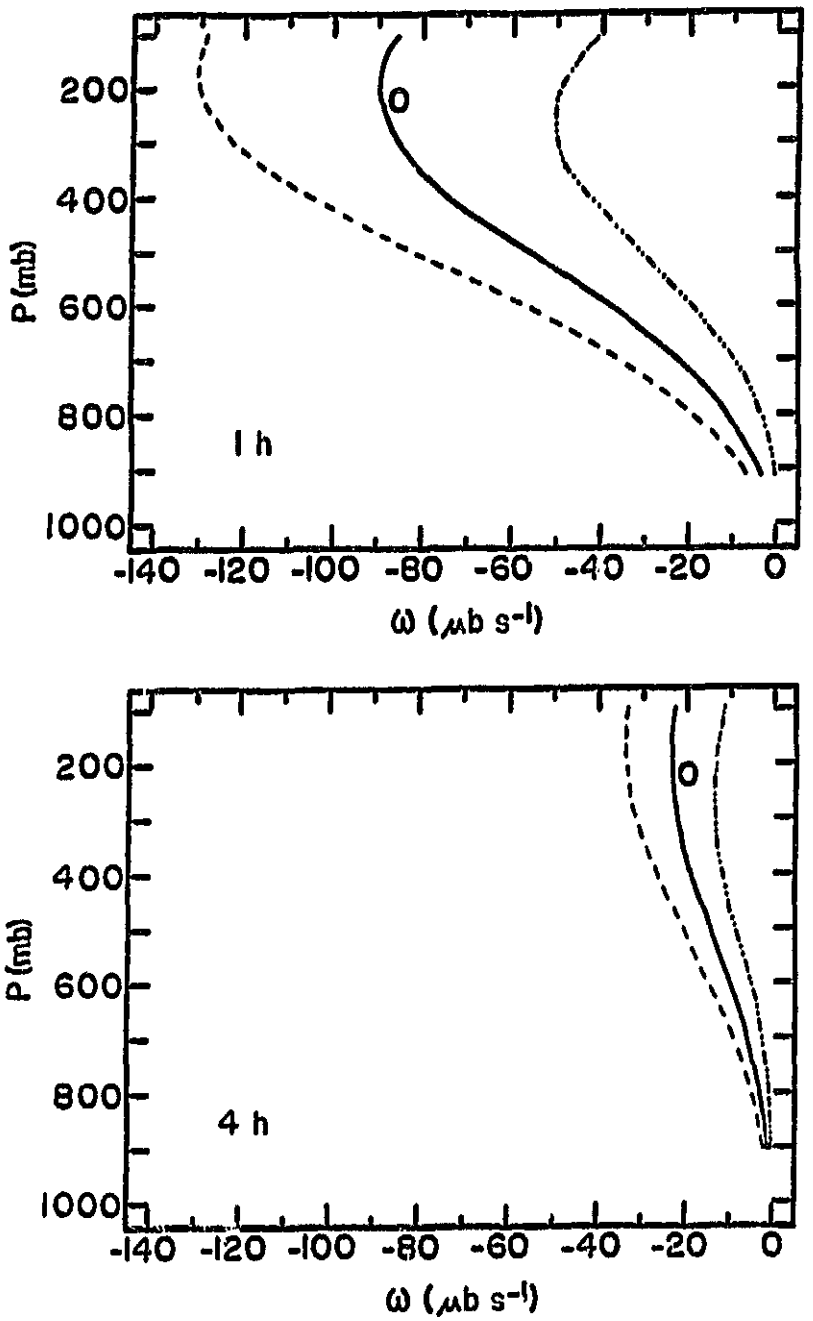

Fig. 10. Vertical motions (μb s^{-1}) from the time derivative component of the vorticity method for 1700 GMT. "0" denotes the observed profile for a grid point over western Wisconsin. The other two curves represent values based on either a +10% (dashed) or -10% (dashed-dot) error in the observed algebraic difference in geostrophic vorticities at each level. For both panels, 1600 and 1700 GMT data were utilized.

considered. In general, VAS-derived patterns show good continuity with those from the traditional source; however, the satellite's values are considerably greater (Fig. 7). At 1200 GMT, upward motion extends from Minnesota to Nebraska; however, at 1300 GMT, the center of ascent over northern Missouri is displaced considerably. By 0000 GMT, the center is along the Iowa-Illinois border, and there is a lobe extending southeastward over a storm area (Fig. 4). VAS adequately fills in the 12 h data gap, showing the eastward progression of rising motion. Thus, capping descent over the future storm area at 1200 and 1300 GMT changes to ascent by 2300 and 0000 GMT. For the subsidence behind the trough, there is agreement over the Northern Plains, but there are discrepancies in the Southern Plains due to $\partial\zeta_g/\partial t$. At 0000 GMT, the descent over Mississippi corresponds to a relative lack of convective activity (Fig. 4). A final point concerns the components of vertical motion. Although the time derivative is dominant for the VAS-derived fields (Fig. 8), the terms are comparable in the case of radiosonde-derived motions (not shown). One should note that 12 h time differences were employed with the RAOB data. Since contributions by geostrophic vorticity advection are very similar for the two sources, it is the greater values of $\partial\zeta_g/\partial t$ that lead to enhanced satellite-derived vertical motion.

Vertical stacking of the satellite-derived motions is depicted in the top cross section of Fig. 11 that passes through the

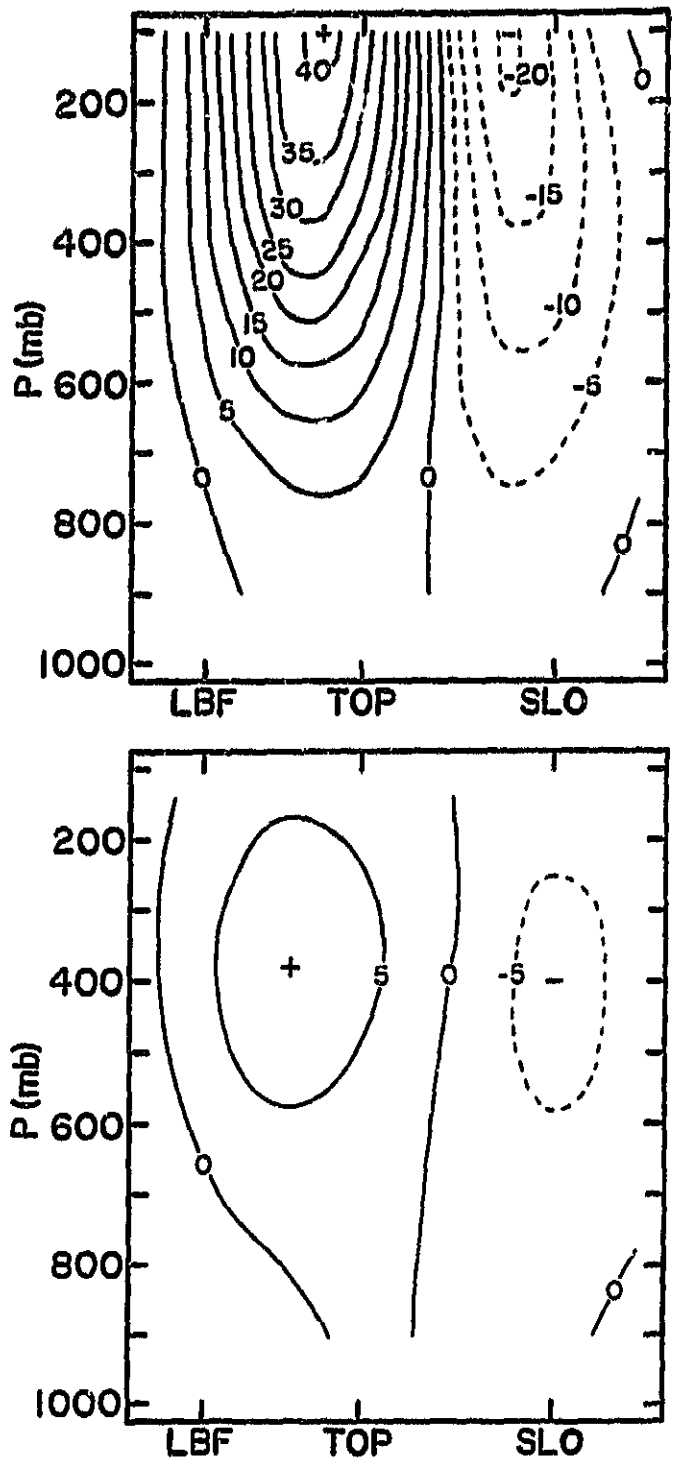

Fig. 11. Cross section of vertical motion (μb s^{-1}) from the vorticity method for 2000 GMT. The axis is shown in Fig. 7; nearby radiosonde sites are indicated. The top profile depicts original values while the bottom contains adjusted values using the O'Brien (1970) technique.

convective outbreak at 2000 GMT (see Fig. 7 for axis). Configurations at each level generally are similar, thereby suggesting that horizontal patterns are comparable to those seen at 600 mb (Fig. 7). This is verified by results at the individual levels (not shown). An unfortunate aspect is that unrealistic motions occur at 100 mb due to the accumulation of error upon vertical integration. To eliminate the problem, the O'Brien (1970) adjustment scheme was applied so that values equaled 0 at 100 mb. This technique has been used extensively with the kinematic method (e.g., Vincent et al., 1976; Smith and Lin, 1978); however, its applicability to the vorticity method has yet to be established theoretically. The resulting profile (bottom of Fig. 11) shows the desired maximum in the middle troposphere. Thus, such an adjustment scheme, is useful when profiles of vertical motions are desired. Of course, it is usually unnecessary near the surface and would not be required in the upper troposphere if only relative magnitudes are needed at each level.

c. Quasi-geostrophic omega equation

The omega equation (4) includes effects of both temperature and vorticity advection. Solutions were obtained using successive relaxation with boundary conditions of $\omega = 0$ at 1000 mb (bottom), 100 mb (top), and on all lateral sides. The constant value for the Coriolis parameter was 0.89×10^{-4} s^{-1}. The lateral boundary condition is a potential source of error. Specifically, systems moving into or out of the region would produce non-zero

values. In the current case, however, the system of interest is well contained within the computational domain. An additional consideration is the stability factor (σ). Values less than zero would produce a hyperbolic formulation with more than one solution instead of the usual elliptical result. This problem does not occur in the current study because σ is always positive. Finally, although data errors may produce hyperbolic solutions, the large scale response function being utilized eliminates this possibility.

Fig. 12 displays vertical motions at 600 mb from both data sources. Continuity between the five VAS-derived fields is excellent. Upward motion is consistently ahead of the trough (Fig. 5) while there is downward motion behind. The center of ascent over Iowa at 1300 GMT advances slowly eastward, extending from Illinois to northern Arkansas by 2300 GMT. Values are greatest at 1700 and 2000 GMT, reaching -2.6 $\mu b\ s^{-1}$ over eastern Iowa, but magnitudes weaken by 2300 GMT. This variation can be explained by the relative contributions of the two equation terms [see (4)]. Although they are complementary near 600 mb, PVA often dominates the ascent at 1700 and 2000 GMT. Since the trough is amplifying (Fig. 5), one might expect greatest uplift at 2300 GMT. Actually, however, due to the orientations of height and vorticity, upward increasing PVA is much weaker, resulting in the smaller ascent. The center of subsidence, due mostly to cold air advection, progresses into northwestern Iowa

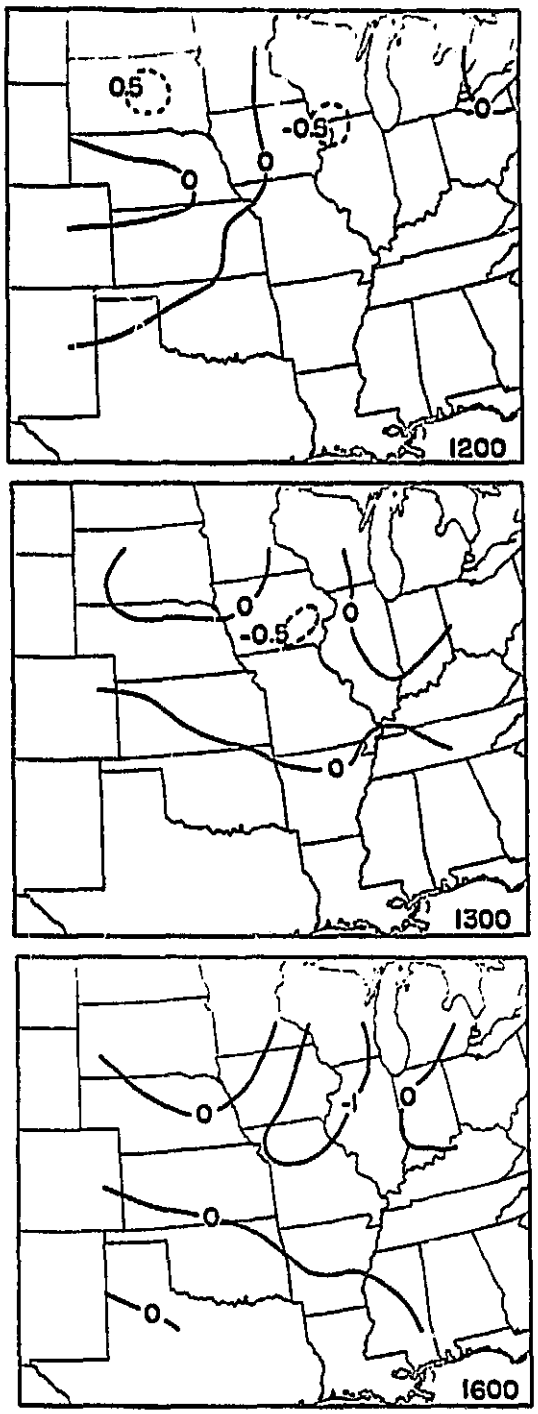

Fig. 12. Vertical motions (μb s^{-1}) at 600 mb from the omega equation. Radiosonde soundings were utilized at 1200 and 0000 GMT while VAS data were employed at the remaining times. The dashed lines at 2000 GMT are axes for the vertical cross sections in Fig. 13.

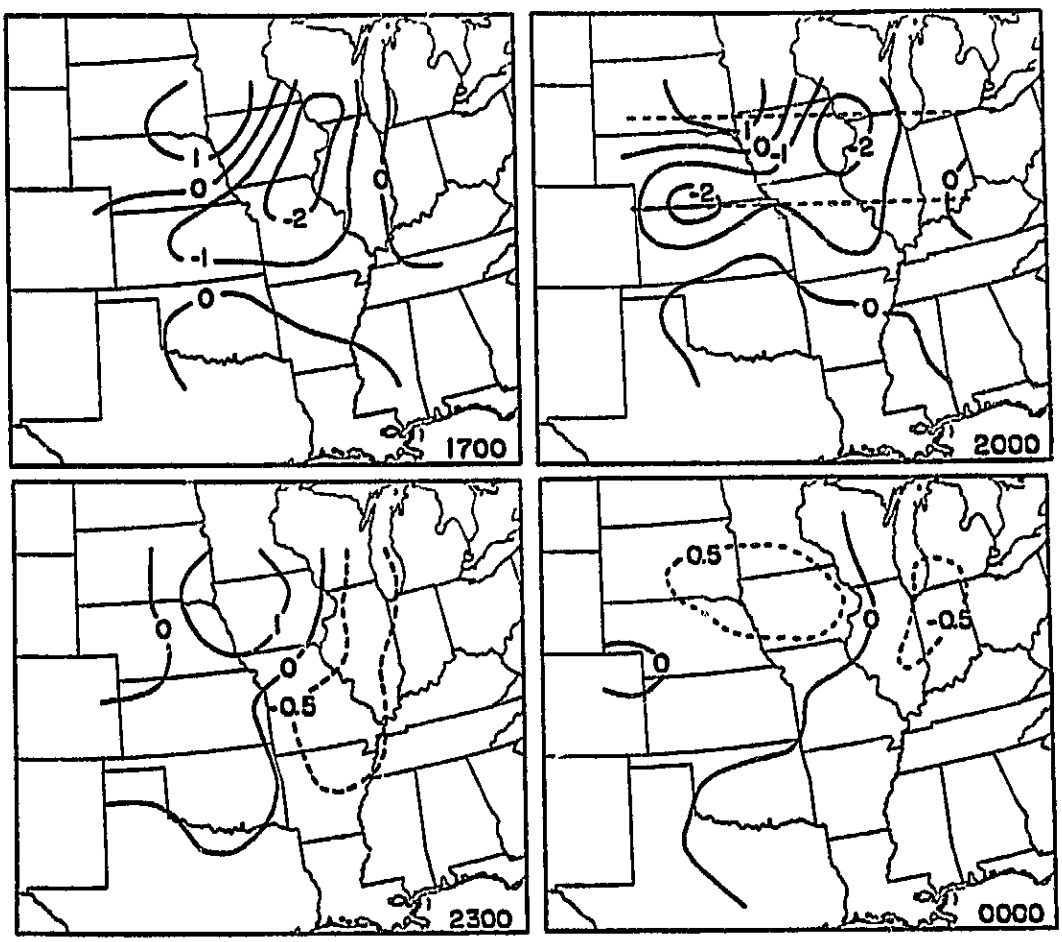

Fig. 12. (Continued)

by 2300 GMT, when magnitudes are greatest. Over the Central Plains, ascent increases through 2000 GMT, but the center is virtually non-existent by 2300 GMT. This feature mostly results from warm air advection which diminishes by 2300 GMT; however PVA is a major contributor at 2000 GMT. Descent over Oklahoma is evident at each time, reaching 1.0 $\mu b\ s^{-1}$ at 1700 GMT. It corresponds to relatively clear skies on the satellite imagery (Fig. 4).

Unlike the vorticity method (Fig. 7), the omega equation does not produce downward motion over Illinois prior to convective development. Instead, weak ascent occurs at each time, although values do become more negative as the trough advances eastward. Once again, it is encouraging that VAS-derived vertical motions diagnose the large scale uplift leading to the convective outbreak.

Major features of VAS-derived vertical motions show remarkable continuity with those from the 12 h radiosonde data (Fig. 12). At 1200 GMT, there is weak ascent ($-0.5\ \mu b\ s^{-1}$) on the border of Iowa, Illinois, and Wisconsin, while weak descent ($0.5\ \mu b\ s^{-1}$) is centered over South Dakota. Satellite-derived patterns at 1300 GMT show similar positions and magnitudes. By 0000 GMT, the negative center extends from eastern Illinois to southern Michigan, while positive values are over Iowa. Corresponding areas at 2300 GMT show close agreement. Finally, weak subsidence over Kansas at 0000 GMT supports the sign reversal between the

final two VAS times. Although VAS data do a very good job of filling in the 12 h gap, the satellite-derived vertical motions generally are larger than those from the sondes. A possible explanation involves the amount of data and its objective analysis. Specifically, even though response functions were identical for both data sources (27% at 800 km), the greater number of VAS retrievals may provide better resolution of the various forcing mechanisms.

Although there is excellent continuity at 600 mb, it is important to consider vertical structure as well. Fig. 13 shows two cross sections at 2000 GMT, the first passing through the main trough and the second through the storm area (see Fig. 12 for axes). Vertical stacking is excellent in each case. For the northernmost diagram (top), ascent and descent are maximized near 600 and 300 mb, respectively. In fact, 300 mb always is the level of maximum subsidence, with greatest values reaching 3.0 $\mu b\ s^{-1}$. Thermal advection is dominant at this level and generally opposes the contribution by vorticity advection. For the southernmost cross section (bottom), regions of uplift associated with the trough and with warm air advection farther west are clearly evident in the lower and middle troposphere. Unlike the vorticity method, excessive values do not occur in the upper troposphere. The cross sections, together with horizontal patterns at other altitudes (not shown), indicate that vertical velocities are reasonable at all levels. Thus, satellite-derived motions

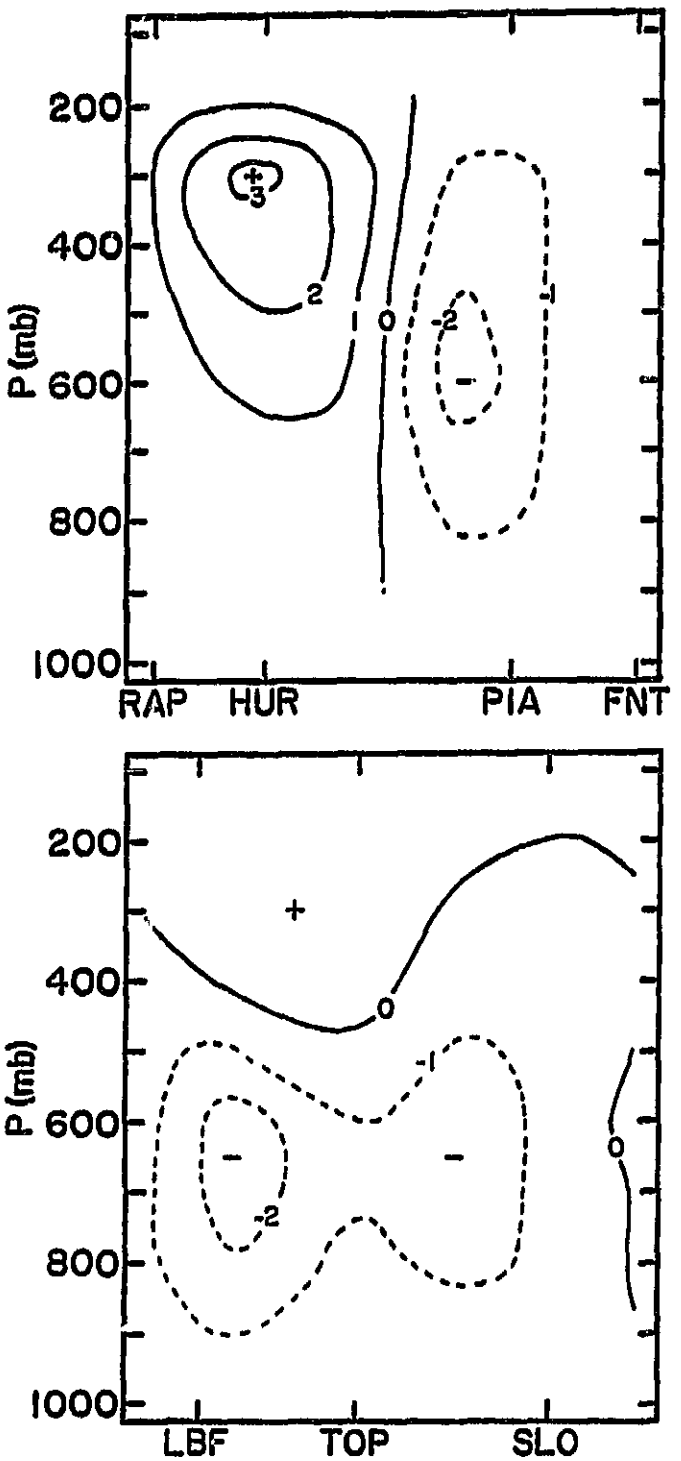

Fig. 13. Cross sections of vertical motion (μb s^{-1}) from the omega equation for 2000 GMT. Axes are shown in Fig. 12; nearby radiosonde sites are indicated.

from the quasi-geostrophic omega equation are very encouraging, giving fields that have good continuity and that bridge the gap between radiosonde data. This is especially significant in light of the data gaps noted earlier (Fig. 1). In terms of magnitude, they correspond to values commonly obtained with NMC forecasting models.

As a final point, vertical motions were re-calculated using a response function that retained 60% of amplitudes at 800 km wavelengths, i.e., the value employed for radiosonde-derived thermodynamic calculations (Section 5-g). The goal was to test the sensitivity of the vertical velocities to smaller scale data features. Fig. 14 contains resulting patterns of height and geostrophic vorticity at 500 mb (top) and vertical motions at 600 mb (bottom) for 1700 GMT. Compared to the original height fields (Fig. 5), the new patterns contain little additional "noise". For vorticity (Figs. 5, 14), magnitudes are substantially altered in the centers, but general patterns and their locations are quite similar. The new vorticity field (Fig. 14) only appears to contain more horizontal detail than the previous version (Fig. 5) because the greater magnitudes lead to an increased number of contours. Finally, patterns of vertical motion from the higher response (Fig. 14) also are very similar to those in Fig. 12, but magnitudes are larger (greatest values at 600 mb are $-5.8\ \mu b\ s^{-1}$ and $4.1\ \mu b\ s^{-1}$, respectively), and centers are more evident. A review of past studies (e.g., Barnes, 1984) suggests that these

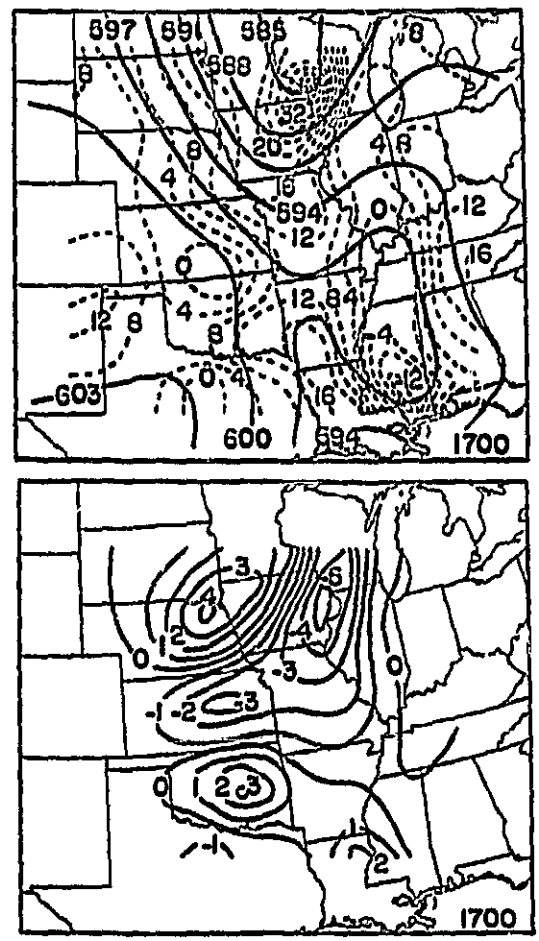

Fig. 14. Heights (decameters) and absolute geostrophic vorticities (10^{-5} s^{-1}) at 500 mb (top), and numerical vertical motions (μb s^{-1}) at 600 mb (bottom) for 1700 GMT. The input data contained a higher response than that used originally in Figs. 5 and 12.

larger values might be inappropriate for the current synoptic weather situation.

The important conclusion is that patterns of numerical vertical motion are not greatly affected by the choice of response parameters. This finding is similar to that of Stuart (1974) who noted that results were not sensitive to the type of analysis technique used to prepare the input height data. On the other hand, patterns from the vorticity method (not shown) were greatly affected by the amount of input detail because of the time derivative and vertical integration. This relative insensitivity to response criteria is an advantage of the numerical procedure. When choosing the parameters, one should consider whether magnitudes of vertical motion are appropriate. However, it is important to note that higher resolution is more likely to violate quasi-geostrophic theory. Therefore, in the current study, the response yielding Rossby numbers near 0.1 was utilized.

d. Adiabatic method

Values from this thermodynamically oriented method depend on atmospheric stability as well as the local change and horizontal advection of potential temperature [see (2)]. Vertical motions were obtained between 800 and 200 mb, but not at 900 mb where diabatic effects usually are quite pronounced. Backward time differencing again was employed to calculate the local time derivative ($\partial\theta/\partial t$), except for forward differencing at 1300 GMT.

Also, since neutral or superadiabatic lapse rates were common over the western part of the analysis region between 700 and 500 mb, potential temperature was required to increase at least 2 K/100 mb (Fuelberg and Lee, 1982) to avoid unrealistically large vertical velocities.

VAS-derived vertical motions at 600 mb are given in Fig. 15. Unlike the presentation for the vorticity method (Fig. 7), the 1700 GMT map was obtained from 1 h differencing; a corresponding diagram based on a 4 h increment will be shown later. Adiabatic motions are not presented for radiosonde data since the adverse VAS-derived patterns to be described below would make objective comparisons impossible. At 1300 GMT (Fig. 15), there is subsidence over virtually the entire region. However, ascent then begins a general westward progression, covering almost the complete domain by 2300 GMT. In other words, there is a sign reversal between the initial and final times. These vertical motions are not associated with the height patterns (Fig. 5). For example, there is no consistent ascent (descent) east (west) of the trough and no satisfactory explanation for the convective outbreak over the middle Mississippi River Valley.

The time derivative causes the unrealistic motions. Components at 1700 GMT (Fig. 16) show that the temporal contribution ($\frac{-\partial\theta/\partial t}{\partial\theta/\partial p}$, top) is at least one order of magnitude larger than that from advection ($\frac{-\vec{V}_2\cdot\vec{\nabla}\theta}{\partial\theta/\partial p}$, bottom). No meteorological process, e.g., temperature advection, adequately explains the abnor-

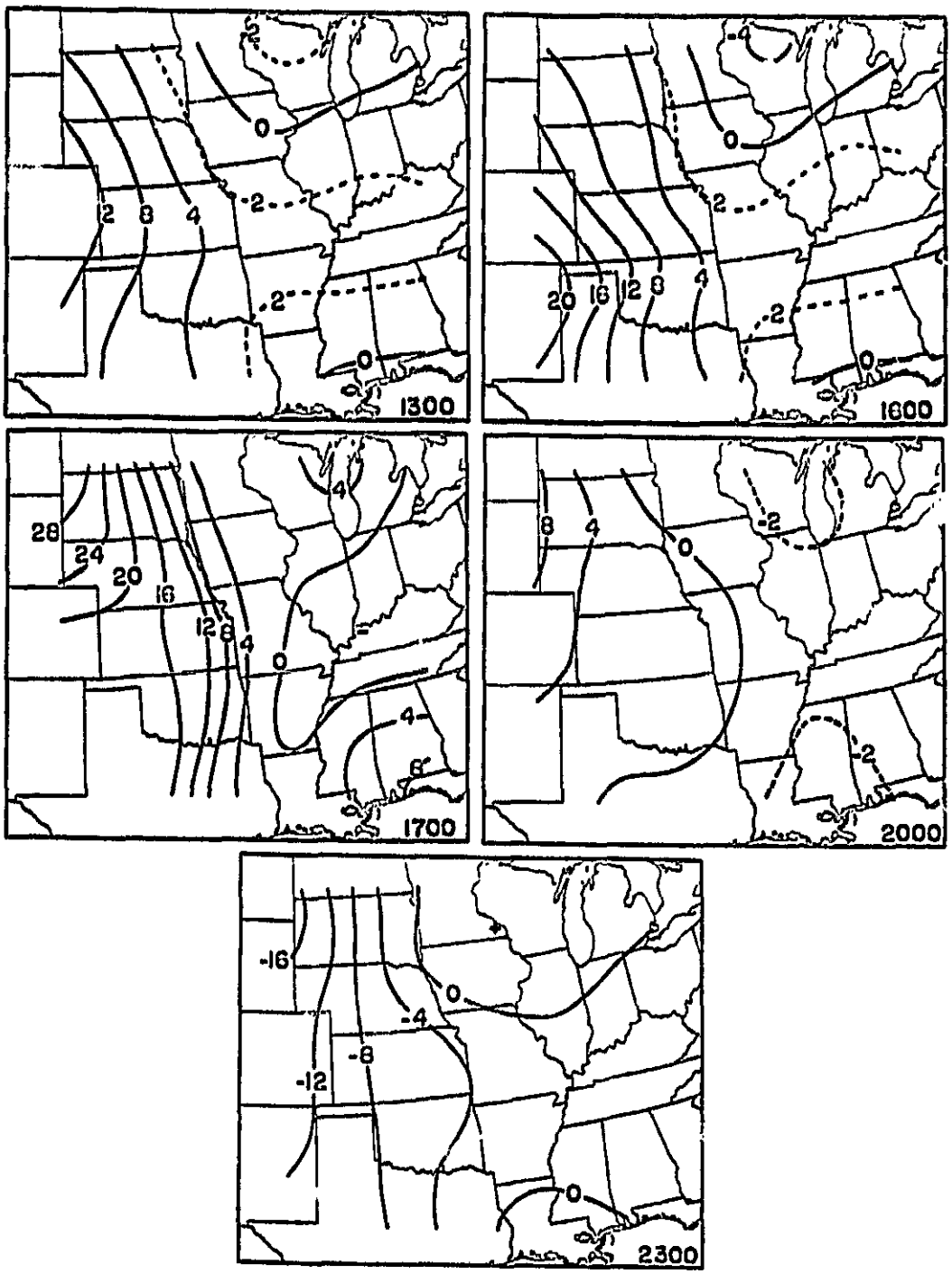

Fig. 15. VAS-derived vertical motions (μb s^{-1}) at 600 mb from the adiabatic method. Patterns at 1700 GMT are from a 1 h time derivative using 1600 GMT data.

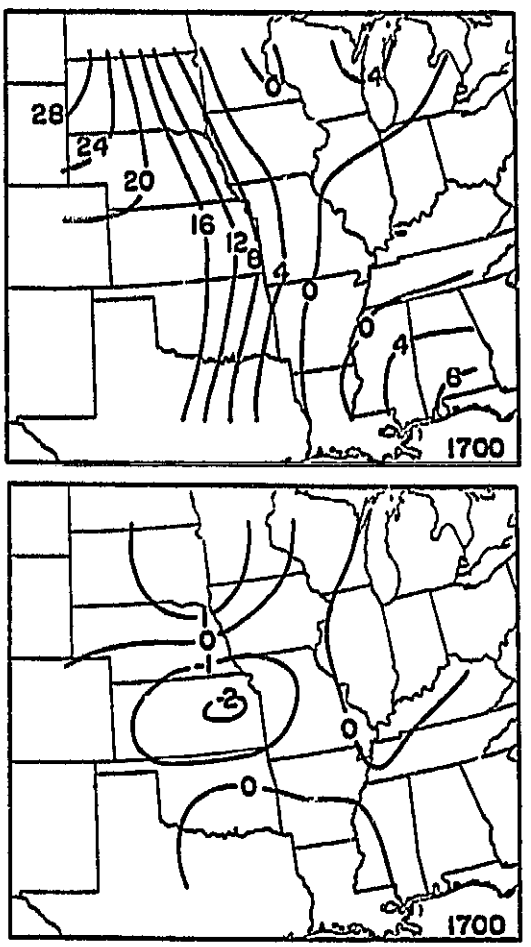

Fig. 16. Temporal ($\frac{-\partial\theta/\partial t}{\partial\theta/\partial p}$, top) and advective ($\frac{-\vec{v}_2 \cdot \vec{\nabla}\theta}{\partial\theta/\partial p}$, bottom) components of vertical motion ($\mu b\ s^{-1}$) from the adiabatic method at 600 mb for 1700 GMT.

mally large middle tropospheric thermal changes causing these motions. After 1700 GMT, thunderstorms might produce low level cooling, and therefore uplift, over the storm region (Fuelberg and Printy, 1983), but, of course, no convection occurs in the other areas. Thus, problems with $\partial\theta/\partial t$ apparently result from diurnal temperature variations. Normally, diurnal effects are confined to the planetary boundary layer, up to about 850 mb. However, the satellite retrievals extend them over too deep a layer, reaching 500 mb at times. These trends are evident in Fig. 17, which is a pressure-time cross section of area averaged temperature ($\overline{T}$) for three subareas of the total analysis region. At 600 mb, there is warming through 2000 GMT in the west (areas 1 and 2), and through 1600 GMT over the storm region (area 3). For example, in subarea 1, $\overline{T}$ increases 1.23°C at 600 mb between 1600 and 1700 GMT, and 2.50°C at 800 and 700 mb. For subarea 2, values are 1.74°C at 600 mb and just over 3.00°C at 800 and 700 mb. Each area, in fact most of the domain, exhibits cooling thereafter. As one expects, the diurnal tendencies are most pronounced nearer the surface.

Based on (2), thermal variability relates directly to vertical motion. Specifically, increases in temperature (and θ) on isobaric surfaces result in descent ($\omega>0$) from $\frac{-\partial\theta/\partial t}{\partial\theta/\partial p}$ since $\partial\theta/\partial p$ is always negative, while decreases in temperature cause ascent. Therefore, over the west, there is subsidence through 2000 GMT (Fig. 15), whereas ascent occurs thereafter. Since this is the

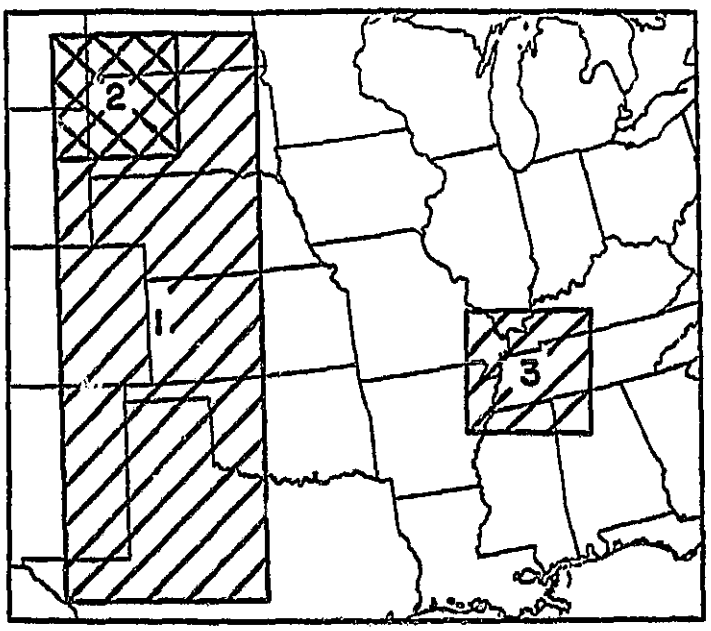

Fig. 17. Pressure-time cross sections of area averaged temperature (°C) (following page) for three subareas of the total analysis region (this page). The number in the upper right corner of each cross section is the number of the subarea on this page. Values are plotted at 600 and 300 mb.

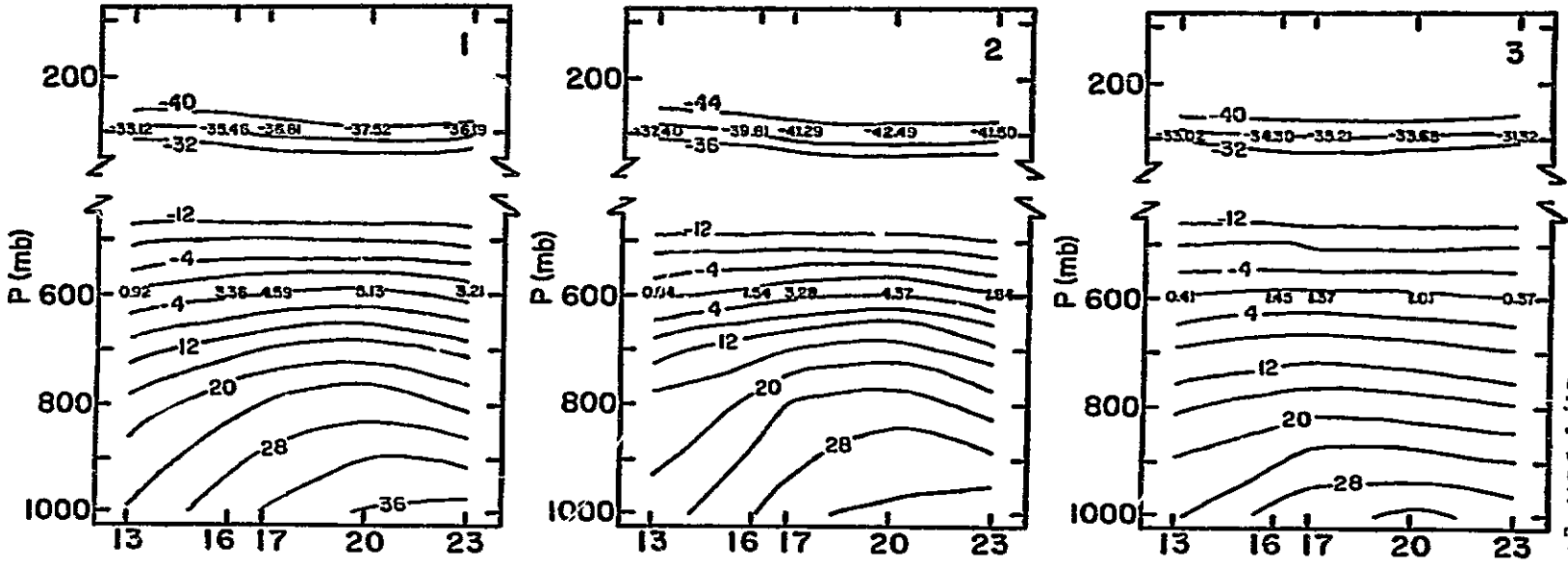

Fig. 17. (Continued)

region of largest diurnal fluctuations and most unstable conditions ($\partial\theta/\partial p$), it is also the area of greatest vertical motions. Based on the requirement that $\partial\theta/\partial p$ increase at least 2K/100 mb, the 1 h warming of 1.74°C in subarea 2 corresponds to average descent of nearly 26 μb s^{-1}. Within the storm region (area 3), warming (Fig. 17) leads to subsidence (Fig. 15) through 1600 GMT, while cooling produces ascent thereafter.

Although the time derivative produces unrealistic patterns, vertical motions from the advection component alone are very reasonable at 600 mb (bottom of Fig. 16). (Note that the contour interval is 1 μb s^{-1} for this map only to insure pattern recognition.) Fields are very similar to those from the Laplacian of temperature advection within the omega equation (not shown). Despite these good patterns, the total fields (Fig. 15) generally do not correspond to the synoptic situation (Fig. 5) because of excessive $\partial\theta/\partial t$.

Based on results from the vorticity method, one might presume that adiabatic vertical motions at 1700 GMT from a 4 h difference (bottom of Fig. 18) would be superior to those from a 1 h interval (Fig. 15). Unfortunately, patterns are very similar to those at 1600 GMT (Fig. 15) since the dominant time derivative was computed from 1300 GMT data in each case. Differences between the two 1700 GMT maps include opposite signs over Wisconsin and different locations for the downward motion over the west. Neither version is consistent with trough/ridge patterns

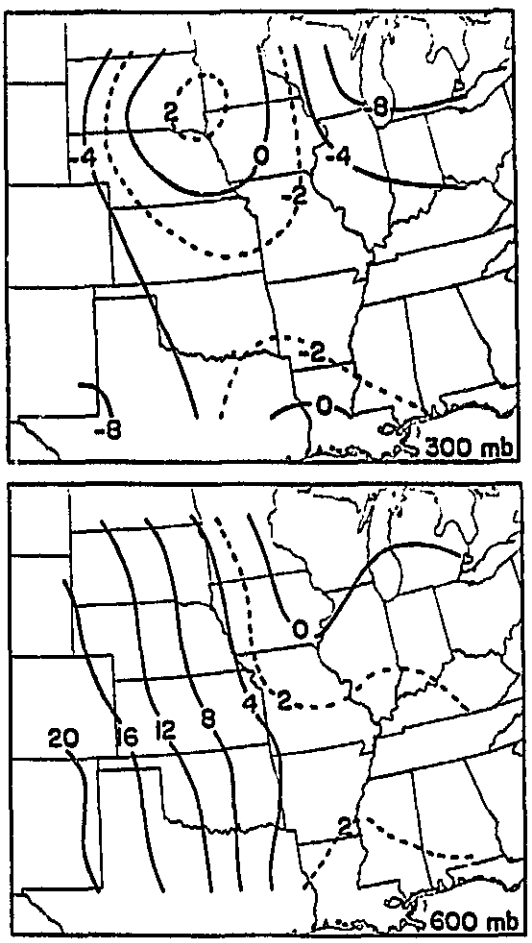

Fig. 18. Vertical motions (μb s^{-1}) at 600 (bottom) and 300 mb (top) for 1700 GMT from the adiabatic method; 4 h time differencing from 1300 GMT data was empl·yed.

(Fig. 5). Concerning magnitudes, values from the 1 h interval generally are more than those from the 4 h version, but this contrast is less than observed with corresponding fields from the vorticity method (Figs. 7 and 9). Thus, it appears that neither 1 h nor 4 h differencing produces satisfactory results; therefore, choice of time intervals is irrelevant.

The apparently fictitious temperature variations produce corresponding height changes (Fig. 5). For example, middle tropospheric heights near the ridge over the Southeast build in response to warming through 1700 GMT, while falls, due to cooling, occur thereafter. Thus, some of the variability in the "capping" ridge near the storm area is due to the apparently erroneous temperatures; however, the radiosonde data (Fig. 5) suggest that part of the decay after 1700 GMT is indeed valid. Similarly, height changes in the western part of the analysis region (Fig. 5) are influenced directly by the diurnal tendencies. However, the shortwave is the primary cause for height variations over the Midwest.

It is important to consider how temperature fluctuations affect vertical motions from the vorticity method. For horizontally uniform fictitious thermal tendencies, the heights would be uniformly altered. Since ζ_g is calculated as the Laplacian of height, its patterns and values would be unaffected. Therefore, both components of the vorticity method (3) also would be unchanged, and the vertical motions would continue to represent

temperature variations due to trough/ridge patterns. On the other hand, thermal tendencies would affect motions from the adiabatic method since temperature variability is considered directly in term $\partial\theta/\partial t$. In the current case, it appears that most of the temperature fluctuations are either relatively uniform over large portions of the domain (e.g., the West) or are dominated by observed meteorological phenomena (e.g., the Midwest). Thus, for the most part, vorticity-derived motions exhibit reasonable continuity (Fig. 7) and are clearly superior to those from the adiabatic method.

Adiabatic vertical motions in the upper troposphere differ considerably from those at 600 mb. Specifically, signs at 300 mb (Fig. 19) generally are the reverse of those below (Fig. 15), as upward motion at 1300 GMT changes to mostly subsidence by 2300 GMT. Again notice the lack of continuity for individual features, e.g., the switch from ascent to descent between 1600 and 1700 GMT over Michigan and Louisiana. The problem, of course, results from unrealistic $\partial\theta/\partial t$. That is, area averaged temperatures (Fig. 17) reveal opposite trends between 600 and 300 mb and the fact that upper tropospheric thermal variations are greatest at this level. For example, early in the period, cooling occurs at 300 mb over the storm area and two western subregions, while warming in all three areas and, in fact, the entire domain occurs thereafter. Thus, for the reasons stated previously, the component of vertical motion due to $\partial\theta/\partial t$, e.g., 1700

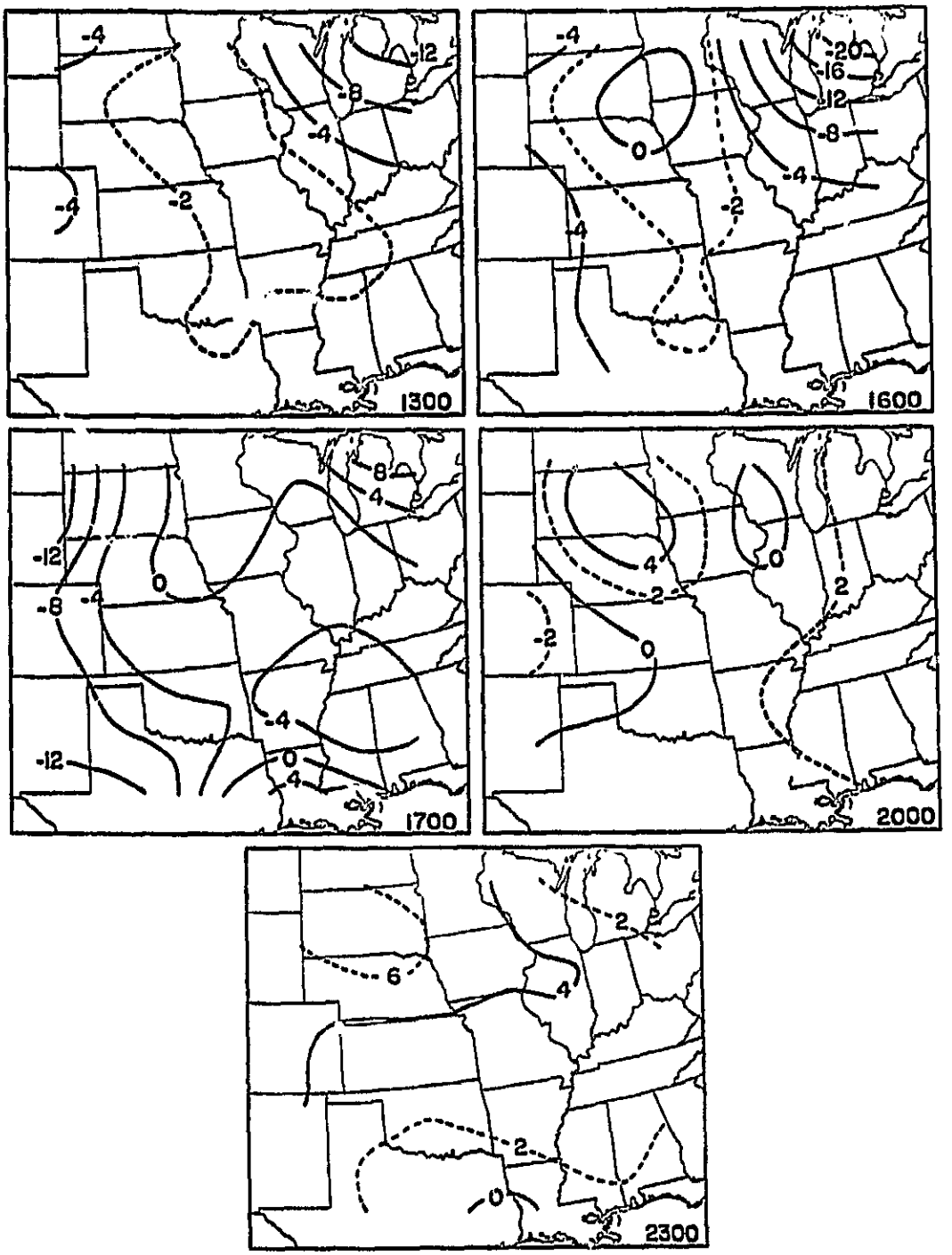

Fig. 19. VAS-derived vertical motions (μb s^{-1}) at 300 mb from the adiabatic method. Patterns at 1700 GMT are from a 1 h time derivative using 1600 GMT data.

GMT (top of Fig. 20), is opposite to that observed at 600 mb (top of Fig. 16).

Local temperature changes at 300 mb also are not related to synoptic features (e.g., horizontal advection). Instead, they apparently result from the physical retrieval algorithm. Specifically, this procedure appears to compensate for excessively deep diurnal effects by producing the reverse situation in the upper levels (W. L. Smith, personal communication, 1985). In the few areas where low level diurnal variations are small and extend over only a shallow layer, there is little or no upper level compensation. Although upper tropospheric fluctuations obviously affect geopotential heights at 300 mb (not shown), low level thermal variations usually dominate. Nonetheless, vorticity-derived motions at 300 mb (not shown) again are greatly superior to the adiabatic versions. Contributions by thermal advection (bottom of Fig. 20) still generally are smaller than those from $\partial\theta/\partial t$ (top), but advection is more important than at 600 mb (Fig. 16), especially at 2000 GMT. Compared to the thermal advection term of the omega equation (not shown), patterns are quite similar; however, values from $-\vec{V}_2 \cdot \vec{\nabla}\theta$ are larger.

Finally, 300 mb vertical motions at 1700 GMT based on a 4 h time interval (top of Fig. 18) are no better than the 1 h version. For example, the 1 h field (Fig. 19) contains large subsidence over Michigan due to warming; however, the 4 h map shows ascent over the same region. Thus, thermal trends over one time

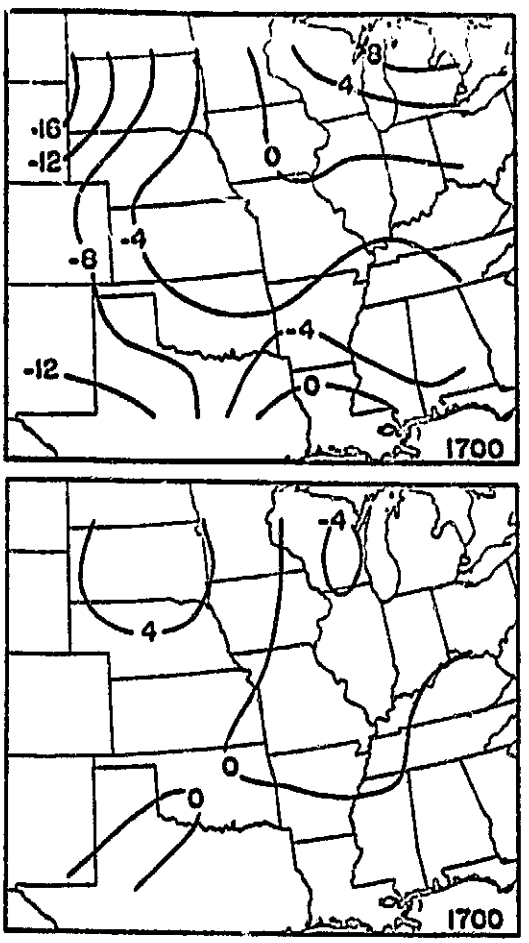

Fig. 20. Temporal ($\frac{-\partial\theta/\partial t}{\partial\theta/\partial p}$, top) and advective ($\frac{-\vec{V}_2\cdot\vec{\nabla}\theta}{\partial\theta/\partial p}$ bottom) components of vertical motion ($\mu b\ s^{-1}$) from the adiabatic method at 300 mb for 1700 GMT.

interval can be quite different from those for a longer period, and unfortunately, the adiabatic technique is very sensitive to these variations. Neither the 1 h nor 4 h versions is acceptable since patterns do not correspond to height configurations (Fig. 5). An attempt was made to minimize the "diurnal effect" by calculating 1700 GMT vertical motions from data at 1300 and 2300 GMT (10 h interval). Unfortunately, the time derivative still is dominant. Thus, results at 600 and 300 mb (not shown) are only slightly improved.

In summary, because of the time derivative, the adiabatic method does not appear to be a promising technique for computing vertical motion from VAS retrievals. Patterns exhibit little relation to synoptic features because implied diabatic effects violate the underlying assumptions of the method. Patterns from the advection component are favorable, and that forcing function is incorporated into the omega equation whose results were quite acceptable.

e. Kinematic method

Past studies of vertical motion (see Section 2-e) generally have considered the kinematic method to be a "standard" against which other procedures are compared. Unfortunately, however, it cannot be applied to satellite-derived data since only geostrophic or gradient winds can be derived thermally. Nevertheless, it is informative to briefly describe general similarities

between radiosonde-derived kinematic motions and versions that are available from VAS.

Fig. 21 shows kinematic motions at 600 mb. At 1200 GMT 21 July, there is descent in the pre-convective environment over southern Illinois, and uplift, associated with the trough (Fig. 5), over eastern Nebraska. By 0000 GMT 22 July, the subsidence moves eastward as ascent advances into Illinois and Indiana. This area extends into Alabama, thereby encompassing the entire region of convective activity (Fig. 4). Also, an area of descent develops over Missouri behind the trough. Identical response parameters (27% at 800 km) were used to analyze both the radiosonde and satellite data; however the kinematic technique is not limited by quasi-geostrophic theory. Therefore, vertical motions also were calculated using a higher response (60% at 800 km). Resulting magnitudes (not shown) are somewhat larger than those in Fig. 21, but patterns are very similar.

Radiosonde-derived motions from the vorticity, numerical, and kinematic techniques should be compared briefly (Figs. 7, 12, 21). At 1200 GMT, the vorticity (Fig. 7) and numerical (Fig. 12) procedures produce areas of ascending and descending motion associated with the trough, while the kinematic method (Fig. 21) shows only the area of ascent. The centers from each technique are displaced from those of the others. Over the future storm region, there is subsidence from all but the omega equation. At 0000 GMT, all three schemes show good agreement for the upward

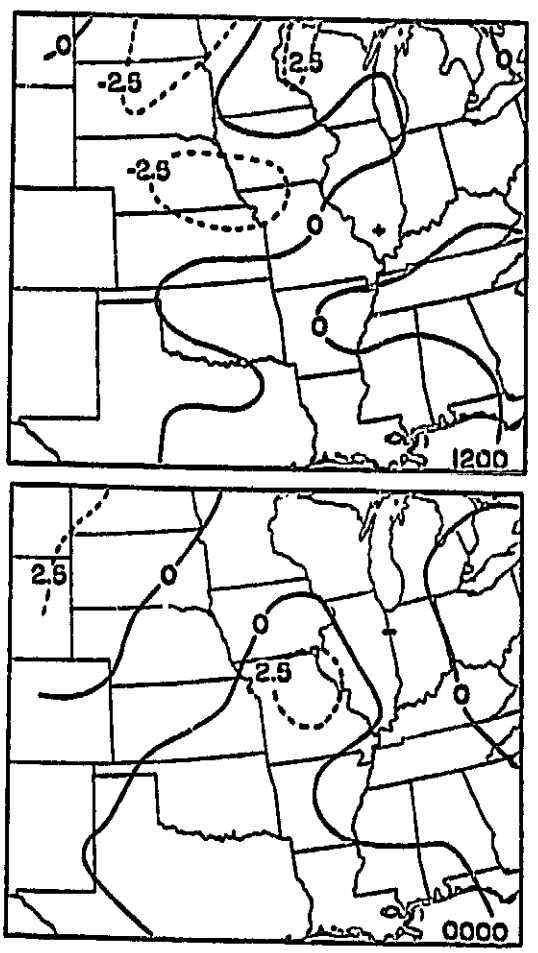

Fig. 21. Radiosonde-derived vertical motions ($\mu b\ s^{-1}$) at 600 mb from the kinematic method for 1200 GMT 21 July and 0000 GMT 22 July.

motion ahead of the shortwave (Figs. 7, 12, 21); however, ascent from the vorticity method is displaced farther west. In addition, each depicts descent behind the trough, although in slightly different locations, and ascent over the convection. Concerning magnitudes, results from the vorticity and kinematic techniques are comparable but are larger than those from the omega equation. In summary, each version is related to the main height features (Fig. 5); moreover, no one procedure is clearly superior.

Details about the individual techniques have been presented in earlier sections; however, it is informative to briefly compare basic features of the kinematic and VAS-derived vertical motions. Only the 1300 and 2300 GMT satellite observations are considered since they are closest to the radiosonde times (1200 and 0000 GMT), and adiabatic motions are not included since results already were shown to be quite poor. With the vorticity method, patterns (Fig. 7) show general agreement with those from the kinematic technique (Fig. 21). Specifically, at the initial times, both versions depict subsidence near southern Illinois and ascent near the trough which, by the final times, also extends over the storm activity (Fig. 4). However, at the end of the period, the downward motion behind the trough shows less agreement, and values are much larger with the vorticity method.

Vertical motions from the omega equation also exhibit similarities with those from the kinematic technique. Specifically,

the main areas of ascent (Figs. 12 and 21), which show only fair agreement at the initial times, have much closer correspondence later in the day. In addition, at the end of the period, both contain descent behind the trough, although in somewhat different locations. Finally, a dissimilarity at 1200-1300 GMT is the area of descending motion that the omega equation does not depict over southern Illinois.

VAS and kinematic vertical motions were compared because kinematic values generally are very reliable. Nonetheless, even that procedure has limitations (see Section 2-a). Therefore, the satellite-based technique that agrees closest with kinematic results is not necessarily superior. Instead, the optimum method will yield vertical motions that 1) correspond most with the height field, 2) show the greatest horizontal and vertical continuity, and 3) best relate and fill in the 12 h gap between radiosonde-derived motions using the same procedure.

f. Comparison of methods

Previous sections qualitatively assessed the individual methods for obtaining vertical motion. This section compares the techniques to one another using both qualitative and quantitative procedures. The first evaluation is to average vertical motions in three key regions: 1) behind, and 2) ahead of the main trough, and 3) over the primary storm area (Fig. 22). "Boxes" 1 and 2 propagated eastward with the trough; however, "box" 3 remained

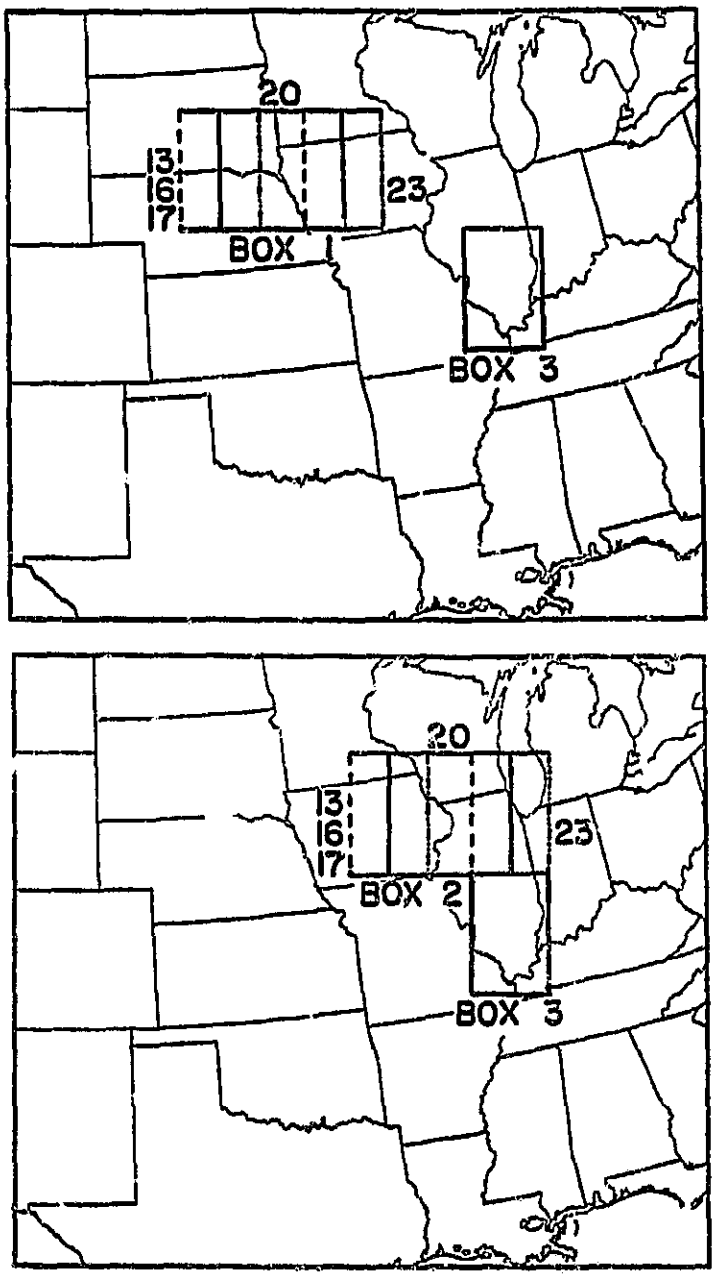

Fig. 22. Areas for which average vertical motions were calculated. At the top, box 1 is behind the shortwave trough, while at the bottom, box 2 is in advance of the wave. Box 3 over southern Illinois is centered over the storm outbreak. Boxes 1 and 2 propagate with the trough although box 3 remains fixed. 13 denotes 1300 GMT.

stationary. The Lagrangian approach for the northernmost boxes depicts the evolution of vertical motions near the developing shortwave. The Eulerian approach for the storm area shows motions prior to and during the convective outbreak. Pressure-time cross sections for the vorticity, numerical, and adiabatic methods are presented for boxes 1-3. The reader is encouraged to review the previous space maps at 600 mb to aid in the comparison (i.e., Figs. 7, 12, 15).

Behind the trough (Box 1, Fig. 23), the vorticity and quasi-geostrophic omega equation provide the most reasonable patterns. (Note that the contour interval is 0.5 $\mu b\ s^{-1}$ for the omega equation but 2.0 $\mu b\ s^{-1}$ for the other methods). Specifically, the vorticity method depicts a gradual transition from ascent to descent during the 10 h period of shortwave amplification, with greatest subsidence at 2300 GMT corresponding to maximum development. Of course, the cross section would be more appealing if an adjustment scheme, such as O'Brien (1970), had been utilized as in Fig. 11. For the omega equation, there is descent in the middle and upper troposphere throughout the period, with greatest values at the final two times. The adiabatic technique offers the least satisfactory patterns. The "diurnal and compensating" effects discussed previously are clearly evident, and there is no trend toward increasing downward motion behind the shortwave.

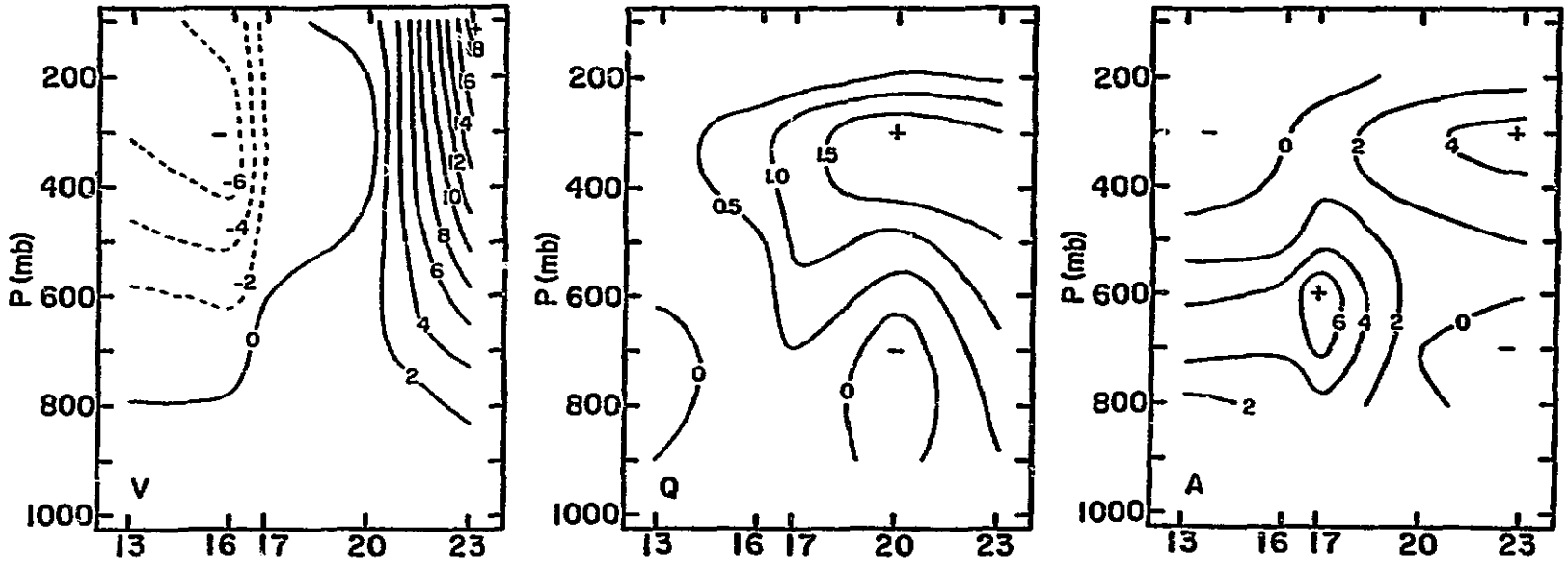

Fig. 23. Pressure-time cross sections of vertical motion (μb s^{-1}) for box 1 (behind the shortwave trough). Values are from "V" the vorticity, "Q" the quasi-geostrophic, and "A" the adiabatic procedures.

East of the trough (Box 2, Fig. 24), the omega equation provides the best results since it consistently shows upward motion that is maximized in the lower and middle troposphere at 2000 GMT. The vorticity method also provides good continuity, except at 2000 GMT. Although horizontal depictions reveal some ascent east of the trough (Fig. 7), the placement of the box at this time mostly captures the larger area of subsidence. An encouraging aspect of the cross section is that values generally peak between 500 and 300 mb without using an adjustment technique. Patterns from the adiabatic technique again are dominated by temporal changes in potential temperature. Therefore, the low level ascent after 1700 GMT is not attributable to the trough.

Finally, over the storm area (Box 3, Fig. 25), the vorticity method yields encouraging patterns. There is descent through 1700 GMT with an abrupt change to ascent thereafter. This result is consistent with the height fields (Fig. 5), the radiosonde-derived vorticity and kinematic motions (Figs. 7, 21), and the timing of the convective outbreak (Fig. 4). Moreover, greatest uplift occurs at 2300 GMT, near the time of maximum convective intensity (Fig. 4). The numerical method also performs well. Although there is no subsidence prior to storm development, weak ascent is maximized in the lower levels at the final two times. Therefore, like the vorticity method, the trend is toward increasing upward motion. Adiabatic values vividly show the effects of diurnal changes in the lower levels and resulting

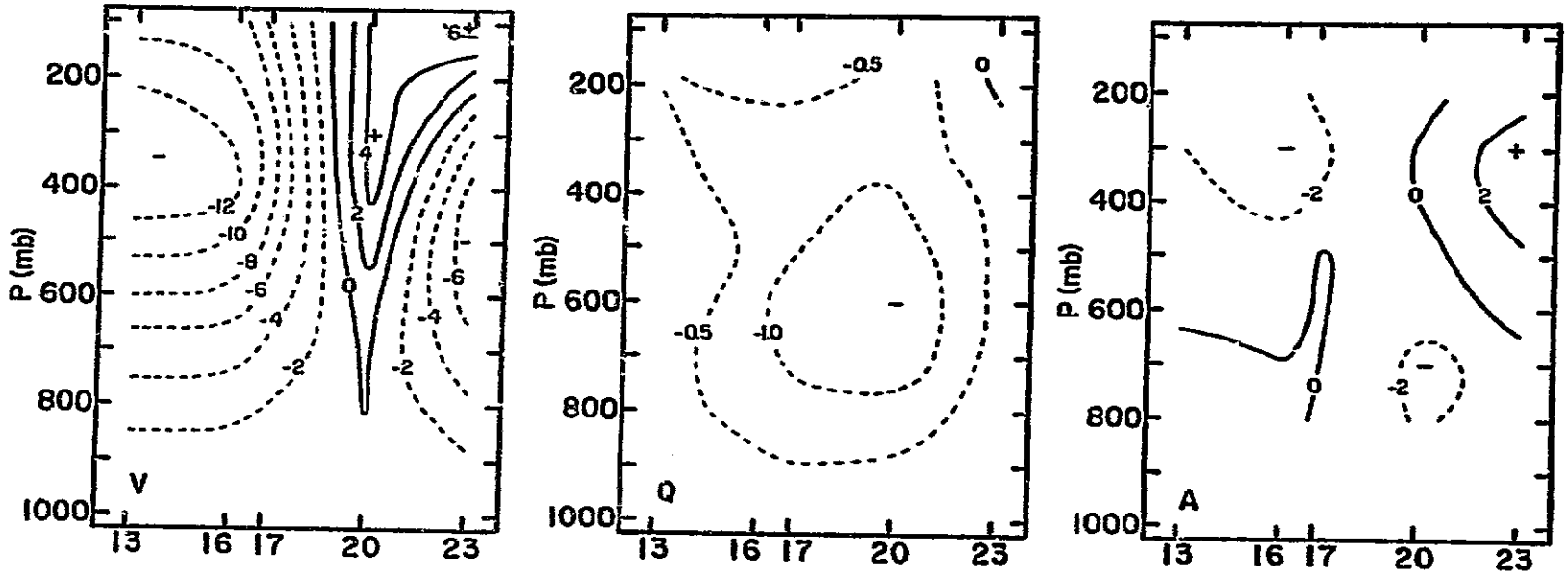

Fig. 24. As in Fig. 23, except for box 2 (in advance of the shortwave trough).

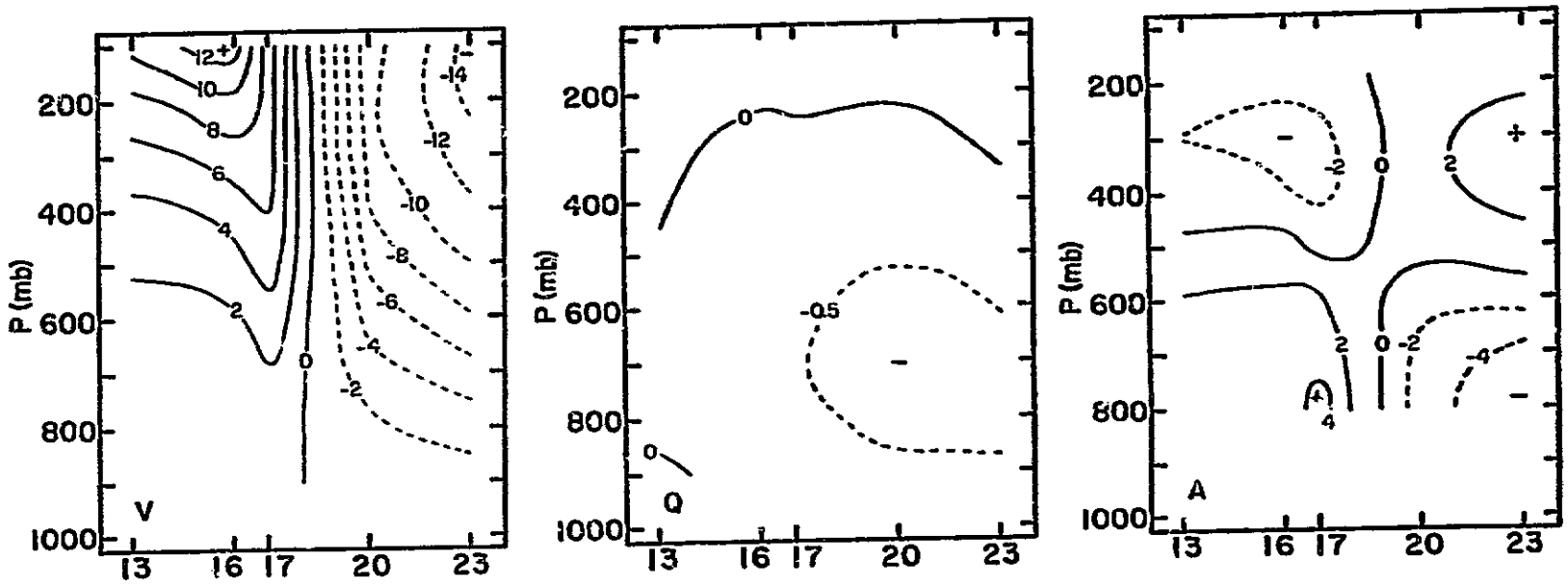

Fig. 25. As in Fig. 23, except for box 3 (the convective region).

compensation aloft. Recalling the horizontal maps (Figs. 15, 19), the cross sectional patterns do not relate to the convective development, despite that appearance in this depiction. As an alternate representation, Fig. 26 contains vertical profiles from the time cross sections in Fig. 25. Notice the abrupt change in vertical velocity from the vorticity method, the gradual increases with the numerical technique, and the variations in the adiabatic scheme attributable to diabatic processes.

In addition to qualitative comparisons, two quantitative assessments of space-time continuity are provided (Chesters et al., 1984): 1) the RMS scale length for gradients within the field at time t, and 2) the temporal correlation between successive fields.

The gradient scale length, L(t), is given by

$$L(t) = [\langle \Delta V^2(t) \rangle / \langle [dV(t)/dx - \langle dV(t)/dx \rangle]^2 \rangle]^{\frac{1}{2}} , \quad (5)$$

where V represents vertical motion at a grid point, $\Delta V(t)$ is given by $\Delta V(t) = V(t) - \langle V(t) \rangle$, and ensemble averages $\langle \ldots \rangle$ are taken horizontally over the entire field. Large L(t) indicates smooth patterns, whereas reduced values depict smaller scale features.

Scale lengths for gradients of vertical motion at 600 and 300 mb are given in Fig. 27. Also included in the left panel are results for absolute geostrophic vorticity at 500 mb (Fig. 5) and, in both panels, the contribution of potential temperature

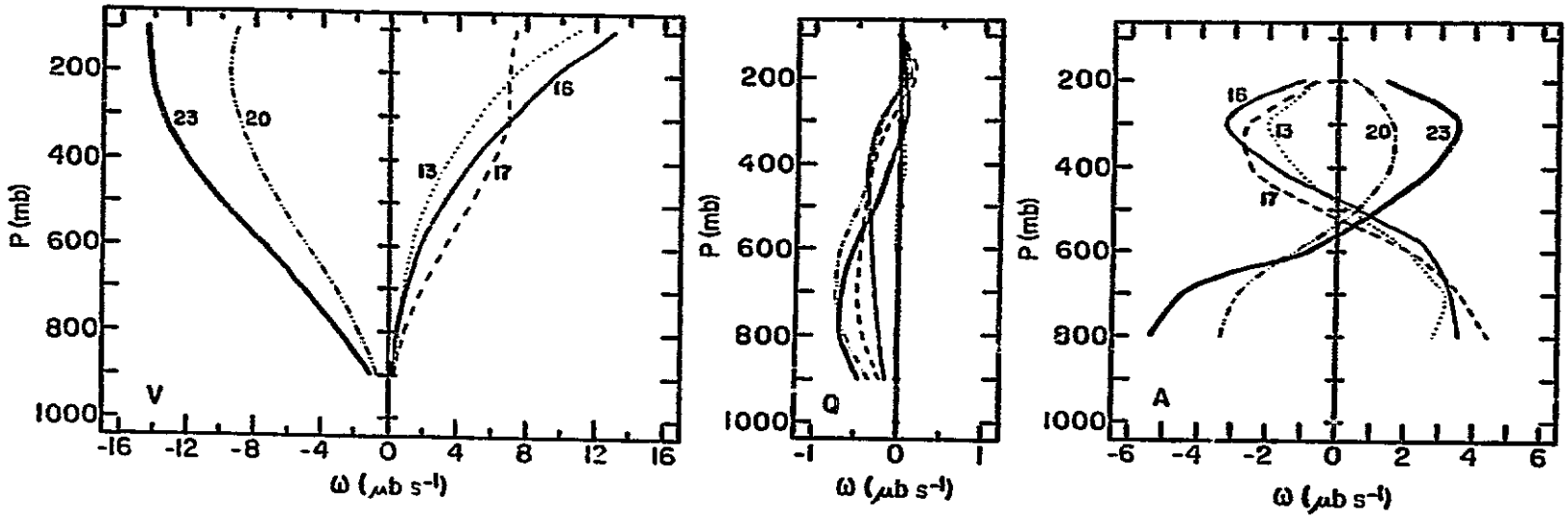

Fig. 26. Vertical profiles of area averaged vertical motion (μb s^{-1}) for box 3 (the convective region). The five VAS times are indicated, and "V", "Q", and "A" are as in Fig. 23.

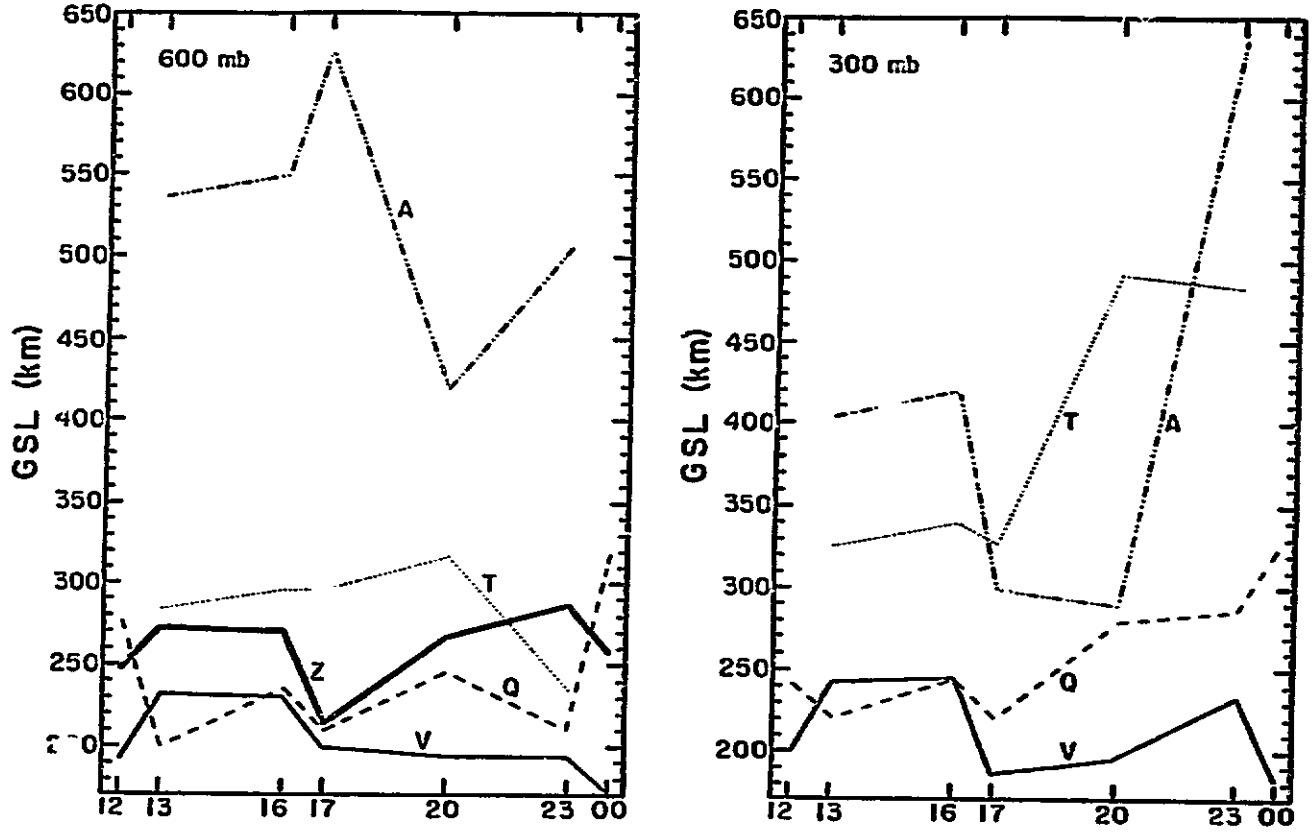

Fig. 27. RMS scale lengths for gradients (GSL) of vertical motion at 600 and 300 mb. Scale lengths are for "V" the vorticity, "Q" the quasi-geostrophic, and "A" the adiabatic methods, while "T" denotes results from the thermal advection term of the adiabatic method. On the panel for 600 mb, "Z" represents results of absolute geostrophic vorticity at 500 mb.

advection in the adiabatic technique. At 600 mb, patterns from the quasi-geostrophic omega equation generally are smoother than those from the vorticity method. This contrast is most pronounced at the two times utilizing radiosonde data (1200 and 0000 GMT) when the difference averages 116 km. The amount of detail provided by either scheme does not change greatly during the 12 h period, a fact readily verified by the horizontal depictions (Figs. 7, 12). An interesting point is that scale lengths of VAS-derived geostrophic vorticity are somewhat greater (smoother patterns) than results from the omega equation or vorticity method. This is expected since derivatives of vorticity influence the vertical motions. Finally, adiabatic motions are by far the smoothest. Scale lengths of its advection component are more similar to those of the other parameters, thereby confirming that total fields are controlled by the time derivative.

Results at 300 mb (Fig. 27) generally are similar to those at 600 mb. For example, patterns from the omega equation again generally are smoother than those from the vorticity method. A marked difference, however, is that scale lengths for the adiabatic method are considerably smaller than at 600 mb (except at 2300 GMT), whereas they are larger for temperature advection. The greater detail in upper level adiabatic motions, especially at 1700 and 2000 GMT, results from the increasing importance of horizontal advection. Nonetheless, earlier sections demonstrated that patterns from this procedure were not related to synoptic

features.

As a second effort to quantitatively assess continuity, temporal correlation coefficients were computed. The defining equation is (Chesters et al., 1984)

$$C(t,t') = \langle \Delta V(t) \Delta V(t') \rangle / [\langle \Delta V^2(t) \rangle \langle \Delta V^2(t') \rangle]^{\frac{1}{2}} , \quad (6)$$

where t and t' are the two observation times. In general, high correlations indicate a continuity of patterns; however, results can be misleading. For example, meteorologically significant but rapidly propagating features can produce small or even negative correlations, whereas slower propagation in an unrealistic direction can yield large values. To further complicate matters, the time intervals being tested are not constant but range from 1 to 3 h. Thus, the coefficients have limited usefulness, but unfortunately, no other statistic appears to provide a more meaningful evaluation.

Figure 28 presents correlation coefficients for 600 and 300 mb. Geostrophic vorticity at 500 mb (bottom panel) shows consistently high correlations, indicating good temporal continuity. Thus, a major input to the vorticity and numerical schemes shows a reasonable propagation of features (also see Fig. 5). With the vorticity method, two of the values at 600 mb are misleading. For the 1300-1600 GMT comparison, the value 0.99 is due to the dominance of the time derivative component, which, as noted earlier, was the same in each case. On the other hand, the negative

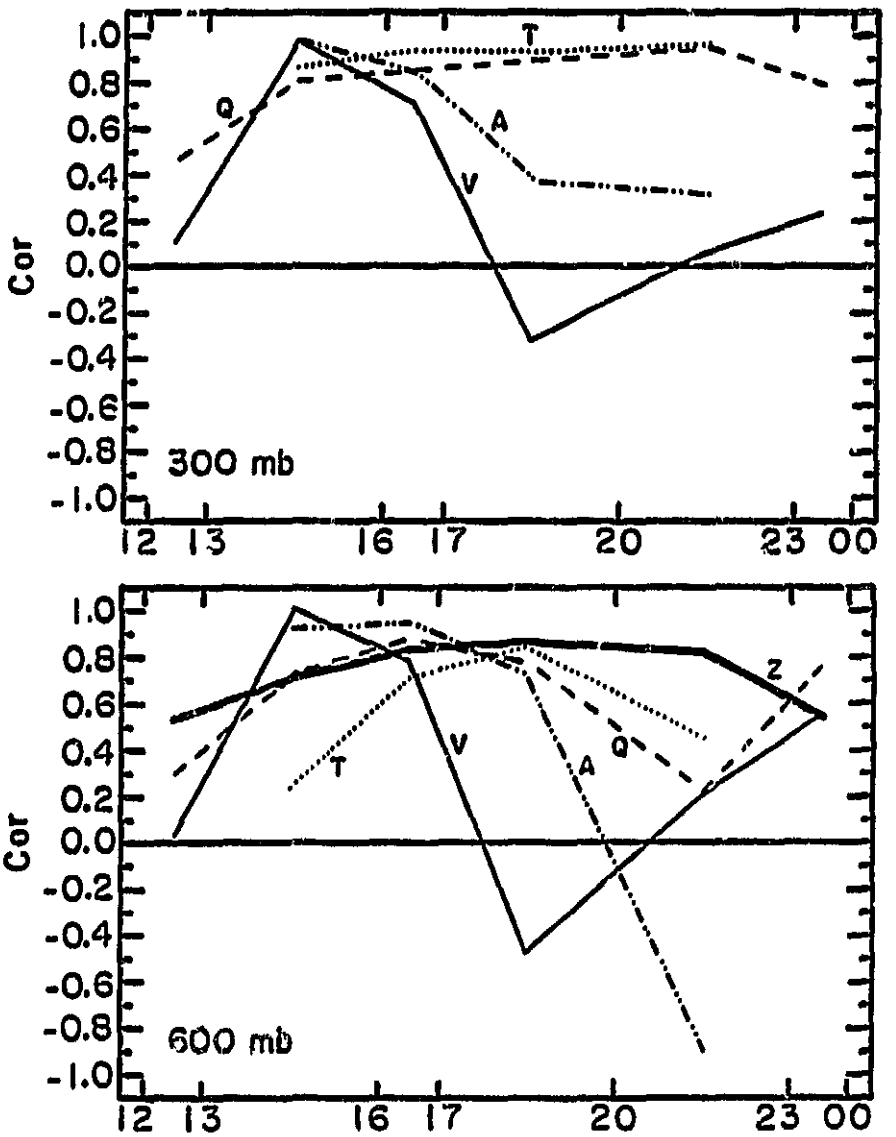

Fig. 28. Temporal correlation coefficients of vertical motion at 600 and 300 mb and absolute geostrophic vorticity ("Z") at 500 mb (bottom). Abbreviations are as in Fig. 27.

value for 1700-2000 GMT reflects rapidly propagating but continuous horizontal patterns (Fig. 7). The omega equation generally exhibits high correlations at 600 mb, except for 2000-2300 GMT (see Section 5-c for reasons). For both the vorticity and numerical methods, there are low correlations between 1200 GMT radiosonde- and 1300 GMT VAS-derived patterns, but values are considerably higher at the 2300-0000 GMT pairing, when the shortwave is better developed and more fully contained within the computational region. Correlations for the adiabatic method initially are high at 600 mb, but this is misleading since they represent good continuity among erroneous features. The value -0.88 between 2000-2300 GMT, reflects the sign reversal in vertical motion. Results for temperature advection range between 0.24 and 0.85. Correlations at 300 mb (Fig. 28) generally are similar to those below; however, a notable exception is the 2000-2300 GMT value from the omega equation. Moreover, adiabatic motions, although generally unrealistic, have a higher correlation between 2000-2300 GMT because the advection component is as influential as the time derivative.

g. Thermodynamic factors

As stated in Section 1, three ingredients are required for thunderstorm formation: instability, moisture, and a triggering mechanism. For the convective outbreak of 21 July, the shortwave trough has been shown to produce large scale ascent over the middle Mississippi River Valley. The temporal and spatial evolution

of the two thermodynamic factors now is considered.

Figure 29 presents radiosonde-derived Lifted Indices (LI) at 1200 GMT 21 July and 0000 GMT 22 July, as well as VAS-derived indices from 1600-2300 GMT. Information concerning the response characteristics of the input data was given in Sections 3-b and c. For the special times, instead of using surface data provided with the VAS retrievals, high density hourly reports from the airways network were employed. Thus, the calculations utilized the greatest amount of surface data possible. Indices at 1200 and 0000 GMT were computed according to the standard definitions; however, values from 1600-2300 GMT were based on a technique developed at the National Severe Storms Forecast Center (Hales and Doswell, 1982). In this procedure, mean boundary layer data are not used; instead, surface parameters are assumed to represent the entire layer during that part of the day when it is well mixed. Since this assumption would not be valid in the early morning, "surface LIs" were not calculated at 1300 GMT.

At 1200 GMT (Fig. 29), strongly stable conditions are over Michigan while lower values cover the midsection of the United States, especially along the Missouri-Illinois border. By 1600 GMT, the entire analysis region apparently is less stable; however, most patterns are similar to those seen earlier. An exception is the lobe of relative stability over Missouri which is due to a pocket of drier air at the surface (not shown). Values continue to decrease over the Mississippi River Valley through 2000

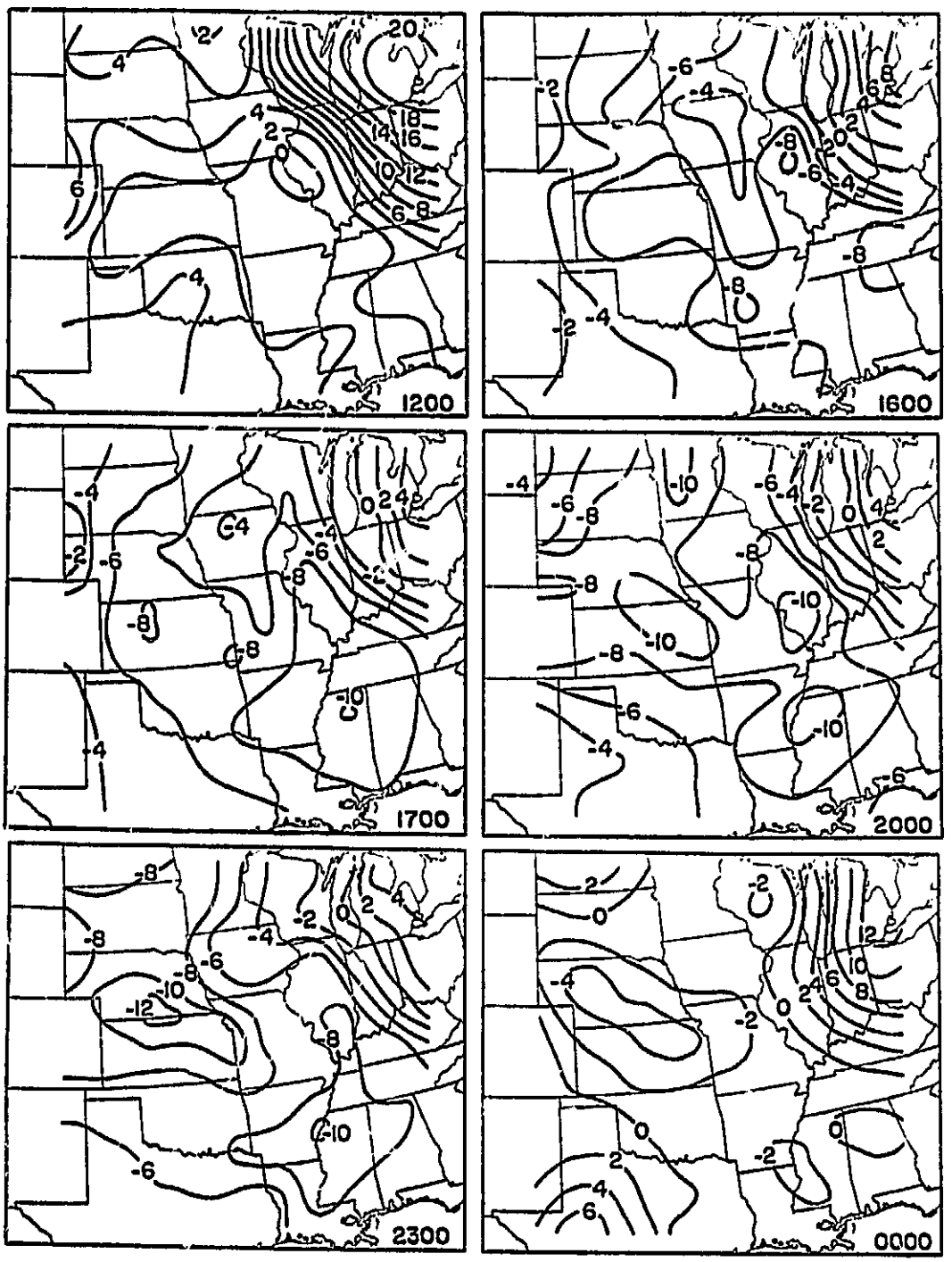

Fig. 29. Radiosonde- (1200 and 0000 GMT) and VAS-derived Lifted Indices. For all times, surface data were from ground based observations.

GMT, reaching a minimum less than -10 over southwest Illinois and northern Mississippi. Growing instability also is depicted over the Central Plains. By 2300 GMT, conditions begin to stabilize from Illinois to Mississippi, although indices continue to decrease over Kansas and Nebraska where convection begins after the study period. Finally, at 0000 GMT, conditions appear to be more stable than 1 h earlier. When interpreting VAS-derived stability indices, it is important to emphasize patterns and trends rather than specific values. This is necessary because a very unstable index based on radiosonde data may be a common occurrence with VAS retrievals, thereby suggesting that a different set of criteria must be employed. Further research is needed to establish these values. Anthony and Wade (1983) observed that VAS-derived stability parameters were less stable than sonde-derived versions although patterns and trends were comparable.

The trend toward increasingly negative LIs over the Mississippi River Valley through 2000 GMT certainly supports the convective outbreak. However, an interesting question is the proportion of these variations that is due to the hourly surface data versus that part attributable to the satellite's 500 mb temperatures. To answer this question, new Lifted Indices were computed from 1600-2300 GMT (Fig. 30). Although the surface data were identical to those employed previously, radiosonde-derived 500 mb temperatures for 1200 GMT were used at each of the four

Fig. 30. Lifted Indices using 1200 GMT radiosonde-derived 500 mb temperatures at each time along with hourly surface reports.

times. Therefore, differences in trends between the two versions of LI will be attributable only to the changing 500 mb temperatures provided by VAS.

Patterns of LI in Fig. 30 are very similar to those in Fig. 29. For example, the most stable air is over the northeast, relatively unstable conditions are over the lower and middle Mississippi River Valley and Central Plains, and a pocket of relatively stable air is in central Missouri. An important point at each time is that values in Fig. 29 are approximately 2 units less than those from the new version (Fig. 30). This difference is caused by VAS's 500 mb temperatures being consistently colder than the 1200 GMT sonde data.

To examine the stability fluctuations, changes in LI (ΔLI) were computed between successive times for each set (Fig. 31). Patterns are very similar, e.g., each depicts negative ΔLI over the storm area through 2000 GMT and increases thereafter. Also, the expansion and enhancement of instability over Kansas and Nebraska through 2300 GMT is found in both versions. Thus, the important conclusion is that VAS's 500 mb data provided little additional information about variations in LI during this case. That is, the sonde's unchanging 500 mb temperatures together with hourly surface reports were sufficient to describe the evolving patterns. It must be emphasized that VAS retrievals would be valuable in those situations having rapid variations in middle tropospheric temperature. Finally, other stability parameters

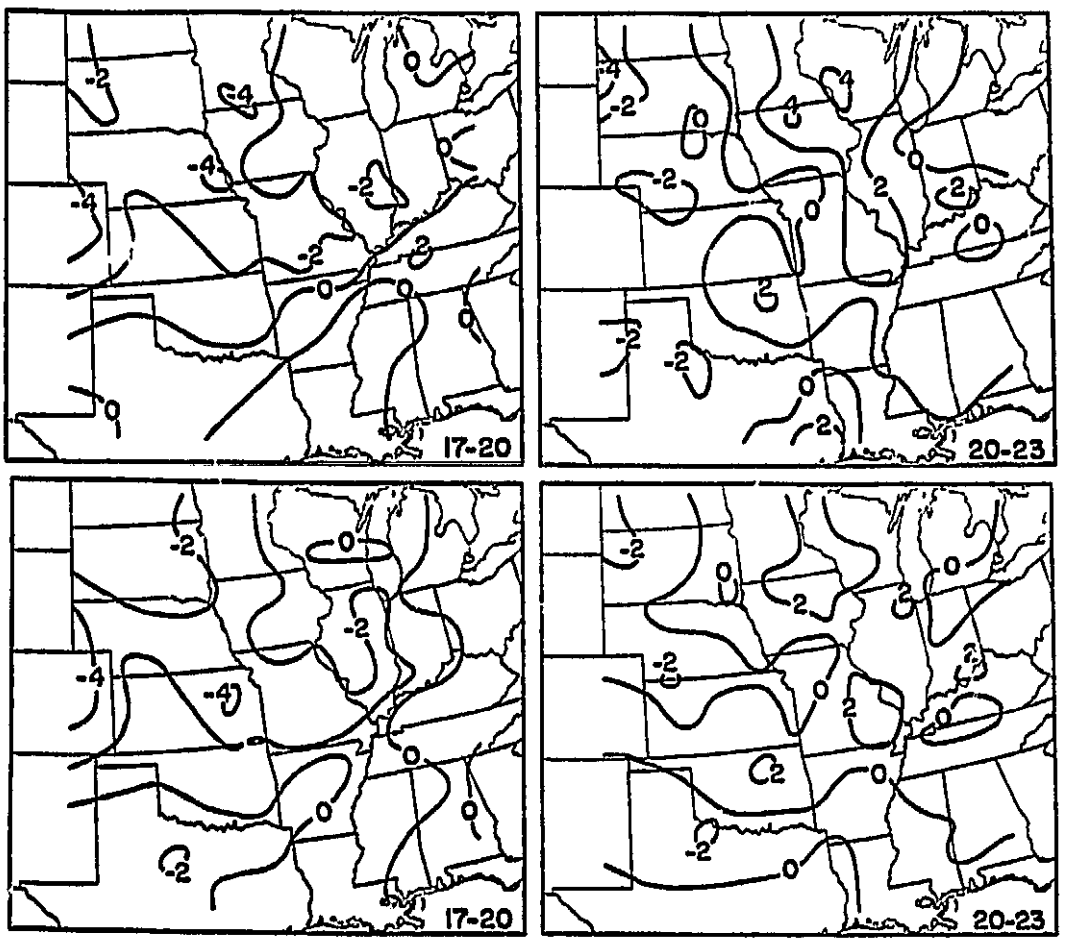

Fig. 31. Changes in Lifted Indices with varying VAS-derived 500 mb temperatures (top) from Fig. 29 and constant radiosonde-derived 500 mb temperatures (bottom) from Fig. 30. 17-20 denotes 1700 to 2000 GMT.

were computed for this case as well, e.g., K Index and Total Totals; however, since their patterns were similar to those of LI, they will not be discussed here. Their agreement indicates that trends at 850 mb were similar to those at the surface. Of course, VAS data would be useful in calculating these indices when conditions at 850 mb were different from surface reports and/or underwent fluctuations between the 12 h radiosonde observations.

The third requirement for thunderstorm initiation is sufficient moisture. Horizontal analyses of surface-300 mb precipitable water from sonde data at 1200 and 0000 GMT and from VAS retrievals between 1300-2300 GMT are presented in Fig. 32. At 1200 GMT, a moist region extends from Minnesota to the Gulf Coast, and VAS-derived patterns at 1300 and 1600 GMT generally continue this feature. Between 1600 and 1700 GMT, just prior to the convective outbreak (Fig. 4), moisture content increases greatly (10 mm) over the lower Mississippi River Valley (Fig. 33). However, from 1700 to 2000 GMT (Figs. 32-33), there is a corresponding decrease over the same region that continues through 2300 GMT (Fig. 32). As noted for stability, patterns and trends of precipitable water probably should be emphasized rather than specific values.

Although the values depict a favorable trend in relation to the storm outbreak, the variations are quite large. Hillger (1984) noted 4 h changes in precipitable water reaching 11.6 mm,

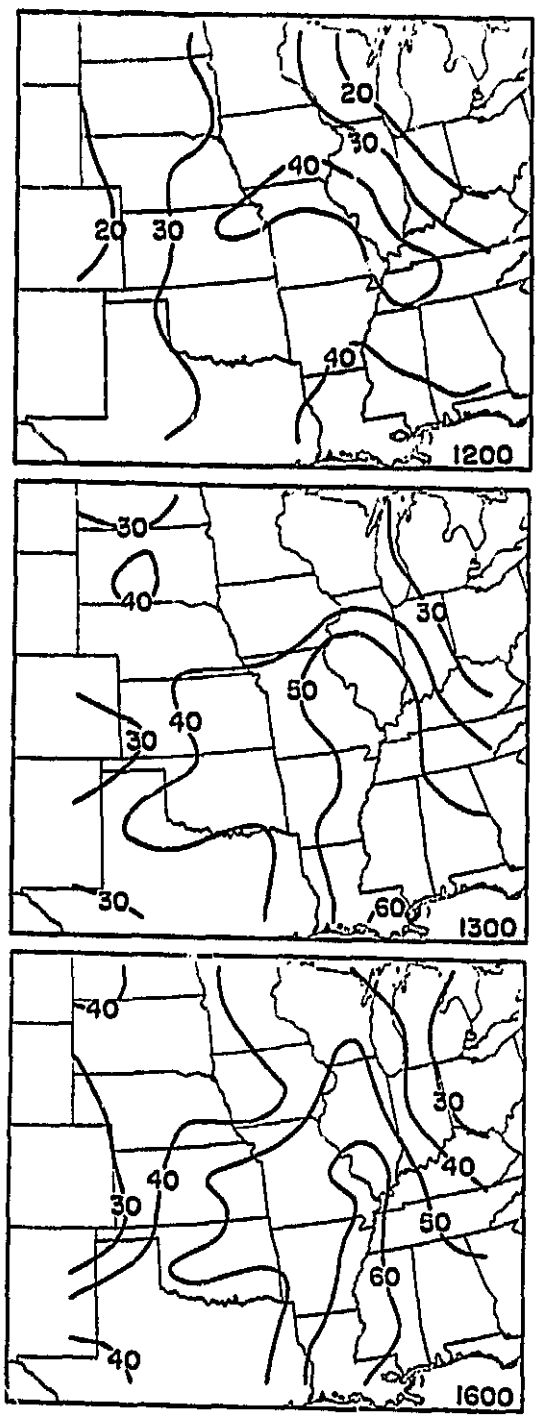

Fig. 32. Radiosonde- (1200 and 0000 GMT) and VAS-derived precipitable water (mm) for the surface to 300 mb layer.

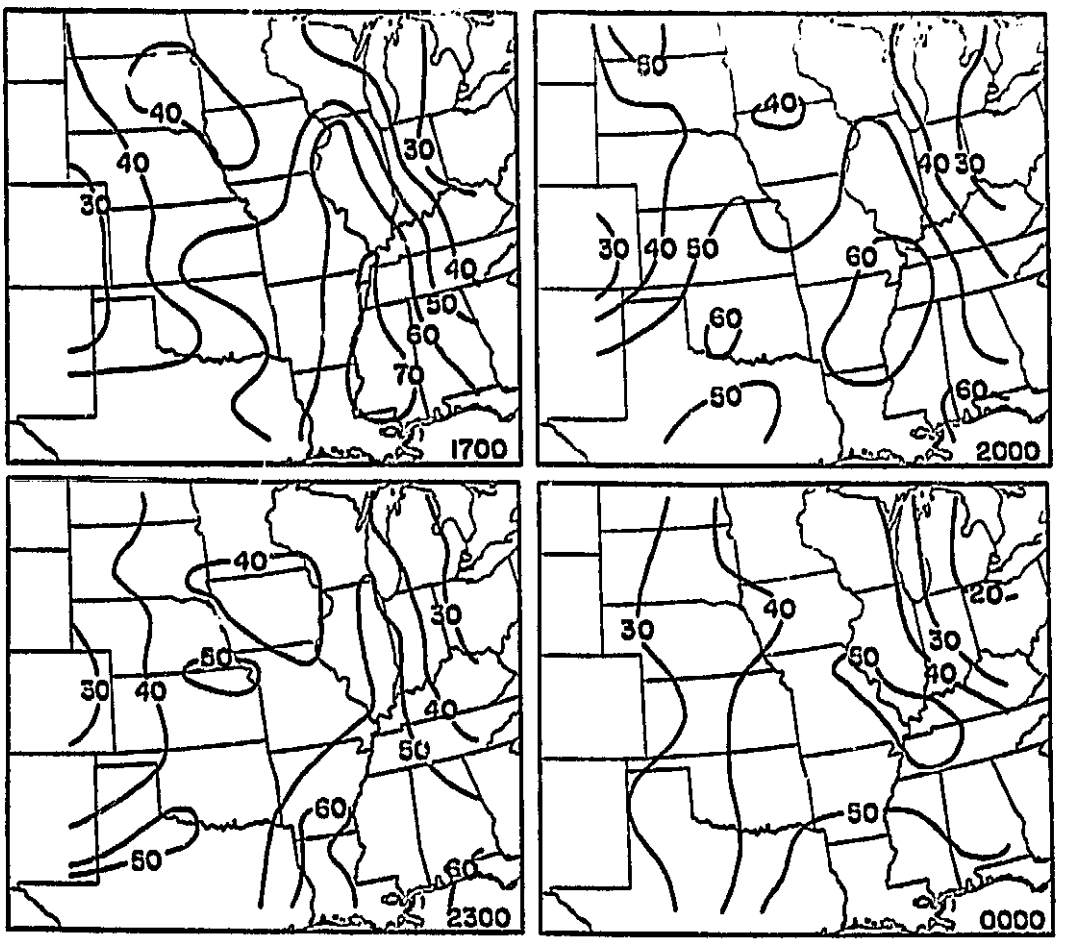

Fig. 32. (Continued)

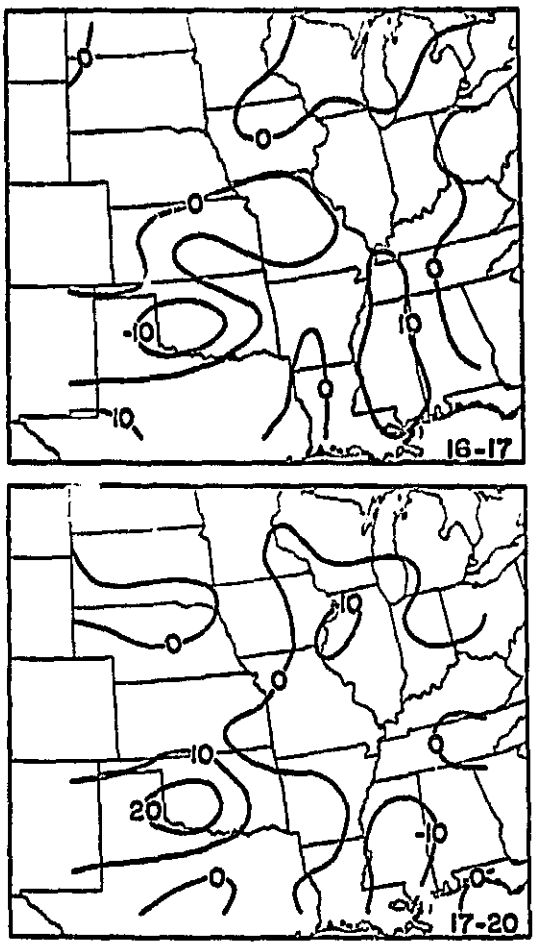

Fig. 33. Changes in VAS-derived precipitable water (mm) for the surface to 300 mb layer. 16-17 denotes 1600 to 1700 GMT.

and he argued their validity on the basis of low level moisture advection and surface moisture convergence. Smith et al. (1981a) observed 3 h fluctuations near 30 mm. In the current study, there is insufficient moisture advection or moisture convergence to explain the 1 h increases of 10 mm. Moreover, surface dewpoints, about 23-24°C (not shown), remain nearly constant from 1600-1700 GMT. Similarly, moisture transport and surface dewpoint fluctuations do not substantiate the decreases in precipitable water between 1700-2000 GMT (Fig. 33). Therefore, the variations must be considered suspect, and they may result from the retrieval algorithm. Recalling Section 5-d, warming below 500 mb (and subsequent height rises) occurred over the area through 1700 GMT, with cooling (and height falls) thereafter. These changes were not confined to the boundary layer. Furthermore, as a result of the deep, unrealistic warming, the retrieval algorithm may have produced increasing precipitable water before the convection with the reverse occurring thereafter (W. L. Smith, personal communication, 1985). However, over the west, in spite of the diurnal temperature fluctuations, there is little variation in precipitable water although that area was much drier originally. Additional research is needed to clarify this relationship. Nonetheless, even though the abrupt changes appear suspect, the overall moist tongue extending along the Mississippi River Valley is quite real since it is verified by radiosonde-derived fields and surface data.

The cause for the convective outbreak now is clear. The shortwave trough caused upward motion that released the energy of the preferentially moist and unstable air over the Mississippi River Valley leading to thunderstorm development near 1735 GMT (Fig. 4). VAS data reveal the three requirements in this area, although there are imperfections in accurately diagnosing each parameter.

6. Summary and conclusions

A case study has investigated the intense convective activity that occurred over the middle Mississippi River Valley on 21-22 July 1982. The goal was to assess the relative strengths and weaknesses of various procedures for calculating vertical motion from VAS satellite retrievals. Magnitudes and continuities of motions from the 1-3 h soundings were evaluated along with their ability to fill in the 12 h gap between radiosonde data. In addition, the study considered the satellite's performance in diagnosing those variations in stability and humidity that were conducive to storm formation. The research benefitted from having VAS retrievals at 1300, 1600, 1700, 2000, and 2300 GMT 21 July. This allowed an examination of conditions prior to and during the thunderstorm outbreak that began shortly after 1700 GMT. For thermodynamic calculations, VAS retrievals were objectively analyzed to achieve meso α-scale resolution of atmospheric structures; however, for vertical motions, only synoptic scale resolution was permitted.

Using the satellite-derived input, the quasi-geostrophic omega equation generally produced the best overall results. These motions exhibited excellent spatial and temporal continuity and consistency with the observed weather. Moreover, they properly bridged the 12 h interval between radiosonde-derived

motions. The vorticity method provided the second best results. Although patterns near the storm area were reasonable, their general continuity and relation to weather events and sonde-derived motions were less favorable. The adiabatic technique produced by far the worst results. Patterns showed poor continuity and had little or no correspondence with synoptic features. Finally, sonde-derived kinematic motions, which served as a general comparison for VAS fields, agreed reasonably with weather conditions.

Poor results from the adiabatic technique occurred because diurnal temperature variations through 600 mb violated the adiabatic assumption. Furthermore, the retrieval algorithm appeared to compensate for the exaggerated diabatic tendencies by producing the opposite effects in the upper troposphere. Thus, vertical motions showed unrealistic patterns and magnitudes because of the time derivative term. Excessively large magnitudes were influenced by the short 1-3 h interval between observations, and values would have been even greater if unrealistic neutral or superadiabatic lapse rates between 700-500 mb had not been suppressed. Adiabatic vertical motions depended directly on thermal fluctuations on individual isobaric surfaces. Therefore, lower tropospheric motions from the time derivative often had no correspondence with those in the upper levels. On the other hand, since the advection component was not based on temperature changes between times, it produced very reasonable patterns.

Results from the vorticity method were much better than adiabatic values because vertical motions depended on the Laplacian of geopotential height that was calculated from vertically integrated temperatures. Therefore, uniform height variations would not affect the vertical motions. In the current case, local vorticity changes were dominated by the presence of the trough/ridge patterns. Since the contribution by advection also was linked to the shortwave, overall vertical motions were appropriate, although magnitudes were quite large, due to the small interval between observations.

The omega equation contains no time derivative; instead vertical motions depend only on fields of temperature and geostrophic vorticity at single times. Since these patterns were very reasonable, both components of ω showed good horizontal continuity. Therefore, the shortcomings of the other two techniques did not apply, and the best overall results were obtained.

Before computations began, it was hoped that the short time interval between satellite observations would improve vertical motions in those methods containing a time derivative. Unfortunately, however, results from the time components were disappointing. Temporal variations in potential temperature did not appear to be meteorologically significant, i.e., they seemed mostly attributable to limitations in the data. Changes in vorticity were more reasonable. Thus, for cases such as 21 July, having data at 1 h intervals apparently will only be useful in

the adiabatic and vorticity techniques when data uncertainties are reduced. In situations of stronger forcing, i.e., a stronger meteorological signal, increased cloud cover likely would limit the number and quality of soundings. Since the numerical method is not as greatly affected by data errors, it appears to be the preferred technique for calculating vertical motions at this time. Its use allows one to take best advantage of the short interval soundings provided by VAS without results being overly influenced by data ambiguities.

Concerning the thermodynamic parameters, the increased frequency of upper air information was not valuable in diagnosing variations in the Lifted Index since fluctuations on 21 July were dominated by surface effects that could be obtained from conventional data. Finally, patterns of VAS-derived precipitable water were similar to those from radiosonde data. The VAS data did reveal rapid changes in magnitudes, but these could not be confirmed on the basis of surface reports.

During this case, VAS provided useful information to supplement the usual 12 h radiosonde soundings. However, only a single case was evaluated, and to the author's knowledge, it was the first to evaluate VAS-derived vertical motions. Therefore, many other periods having a variety of synoptic conditions need to be examined. In addition, a new physical retrieval algorithm has been developed in which excessive diurnal and compensating temperature variations are reduced (W. L. Smith, personal communica-

tion, 1985). Thus, an especially interesting study would be to repeat the current calculations based on the improved soundings. Finally, better procedures for handling data gaps should be developed. In the current case, despite numerous gaps, results did not appear to be greatly affected. Only through such future studies can VAS's ability to provide the mesoscale data needed for improved forecasting be clearly evaluated.

REFERENCES

Anthony, R. W., and G. S. Wade, 1983: VAS operational assessment findings for Spring 1982/83. Preprints Thirteenth Conf. Severe Local Storms, Tulsa, Amer. Meteor. Soc., J23-J28.

Barnes, S. L., 1973: Mesoscale objective analysis using weighted time-series observations. NOAA Tech. Memo. ERL NSSL-62, National Severe Storms Laboratory, Norman, OK 73069, 60 pp. [NTIS COM-73-10781].

_____, 1984: Omega diagnostics as a supplement to LFM/MOS guidance in a weakly-forced convective situation. Preprints Tenth Conf. Weather Forecasting and Analysis, Clearwater Beach, Amer. Meteor. Soc., 147-154.

Chesters, D., L. W. Uccellini, and A. Mostek, 1982: VISSR atmospheric sounder (VAS) simulation experiment for a severe storm situation. Mon. Wea. Rev., 110, 198-216.

_____, T. H. Lee, A. Mostek, and D. A. Keyser, 1984: The accuracy of mesoscale temperature and dewpoint fields retrieved from VAS satellite and conventional surface data. Preprints Conf. Satellite Meteorology/Remote Sensing and Applications, Clearwater Beach, Amer. Meteor. Soc., 226-231.

Collins, G. O., and P. M. Kunn, 1954: A generalized study of precipitation forecasting. Part 3: Computation of precipitation resulting from vertical velocities deduced from vorticity changes. Mon. Wea. Rev., 82, 173-182.

Dutton, J. A., 1976: The Ceaseless Wind: An Introduction to the Theory of Atmospheric Motion. McGraw-Hill, New York, 579 pp.

Eliassen, A., and W. E. Hubert, 1953: Computations of vertical motion and vorticity budget in a blocking situation. Tellus, 5, 196-206.

Fankhauser, J. C., 1969: Convective processes resolved by a mesoscale rawinsonde network. J. Appl. Meteor., 8, 778-798.

Fuelberg, H. E., and M. F. Printy, 1983: Meso β-scale thunderstorm/environment interactions during AVE-SESAME V

(20-21 May 1979). Bull. Amer. Meteor. Soc., 64, 1144-1156.

_____, and W. S. Lee, 1982: A comparison of adiabatic and kinematic vertical motions using mesoscale data. Preprints Ninth Conf. Weather Forecasting and Analysis, Seattle, Amer. Meteor. Soc., 417-423.

Hales, J. E., Jr., and C. A. Doswell III, 1982: High resolution diagnosis of instability using hourly surface lifted parcel temperatures. Preprints Twelfth Conf. Severe Local Storms, San Antonio, Amer. Meteor. Soc., 172-175.

Haltiner, G. J., L. C. Clarke, and G. E. Lawniczak, Jr., 1963: Computation of the large scale vertical velocity. J. Appl. Meteor., 2, 242-259.

Hansen, J., and A. H. Thompson, 1965: Vertical motion calculations and satellite cloud observations over the western and central United States. J. Appl. Meteor., 4, 18-30.

Hillger, D. W., 1984: Spatial and temporal variations in mesoscale water vapor retrieved from TOVS infrared radiances in a nocturnal inversion situation. J. Clim. Appl. Meteor., 23, 704-723.

Holton, J. R., 1979: An Introduction to Dynamic Meteorology. Academic Press, New York, 391 pp.

Hoskins, B. J., I. Draghici, and H. C. Davies, 1978: A new look at the ω-equation. Quart. J. Roy. Meteor. Soc., 104, 31-38.

Koch, S. E., M. DesJardins, and P. J. Kocin, 1983: An interactive Barnes objective map analysis scheme for use with satellite and conventional data. J. Clim. Appl. Meteor., 22, 1487-1503.

Krishnamurti, T. N., and W. J. Moxim, 1971: On parameterization of convective and nonconvective latent heat release. J. Appl. Meteor., 10, 3-13.

Lee, T. -H., D. Chesters, and A. Mostek, 1983: The impact of conventional surface data upon VAS regression retrievals in the lower troposphere. J. Climate Appl. Meteor., 22, 1853-1874.

Menzel, W. P., W. L. Smith, and L. D. Herman, 1981: Visible infrared spin-scan radiometer atmospheric sounder radiometric calibration: An inflight evaluation from inter-comparisons with HIRS and radiosonde measurements. Appl. Opt., 20, 3641-3644.

Miller, A., and H. A. Panofsky, 1958: Large-scale vertical motions and weather in January 1953. Bull. Amer. Meteor. Soc., 39, 8-13.

Moore, J. T., and H. E. Fuelberg, 1981: A synoptic analysis of the first AVE-SESAME '79 period. Bull. Amer. Meteor. Soc., 62, 1577-1590.

O'Brien, J. J., 1970: Alternate solution to the classical vertical velocity problem. J. Appl. Meteor., 9, 197-203.

Pagnotti, V., and L. F. Bosart, 1984: Comparative diagnostic case study of East Coast secondary cyclogenesis under weak versus strong synoptic-scale forcing. Mon. Wea. Rev., 112, 5-30.

Peddar, M. A., 1981: On the errors of kinematic vertical motion estimation using divergence bias adjustment procedures. Mon. Wea. Rev., 109, 1813-1816.

Shuman, F. G., 1957: Numerical methods in weather prediction: II. Smoothing and filtering. Mon. Wea. Rev., 85, 357-361.

Smith, P. J., 1971: An analysis of kinematic vertical motions. Mon. Wea. Rev., 99, 715-724.

_____, and C. P. Lin, 1978: A comparison of synoptic-scale vertical motions computed by the kinematic method and two forms of the omega equation. Mon. Wea. Rev., 106, 1687-1694.

Smith, W. L., 1983: The retrieval of atmospheric profiles from VAS geostationary radiance observations. J. Atmos. Sci., 40, 2025-2035.

_____, C. M. Hayden, H. M. Woolf, H. B. Howell, and F. W. Nagle, 1979: Interactive processing of TIROS-N sounding data. Remote Sounding of the Atmosphere from Space, Pergamon Press, New York, 33-47.

_____, V. E. Suomi, F. X. Zhou, and W. P. Menzel, 1981a: Nowcasting applications of geostationary satellite atmospheric sounding data. Nowcasting, K. A. Browning Ed., Academic Press, New York, 123-135.

_____, V. E. Suomi, W. P. Menzel, H. M. Woolf, L. A. Sromovsky, H. E. Revercomb, C. M. Hayden, D. N. Erickson, and F. R. Mosher, 1981b: First sounding results from VAS-D. Bull. Amer. Meteor. Soc., 62, 232-236.

Stuart, D. W., 1974: A comparison of quasi-geostrophic vertical

motion using various analyses. Mon. Wea. Rev., 102, 363-374.

Tronberth, K. E., 1978: On the interpretation of the diagnostic quasi-geostrophic omega equation. Mon. Wea. Rev., 106, 131-137.

Vincent, D. G., K. E. Bossingham, and H. J. Edmon, Jr., 1976: Comparison of large scale vertical motions computed by the kinematic method and quasi-geostrophic ω-equation. Preprints Sixth Conf. Weather Forecasting and Analysis, Albany, Amer. Meteor. Soc., 357-364.

Wilson, G. S., 1976: Large-scale vertical motion calculations in the AVE-IV Experiment. Geophys. Res. Lett., 3, 735-738.

BIOGRAPHY OF THE AUTHOR

Theodore Wenrich Funk was born on May 3, 1960 in Reading, Pennsylvania. He spent his first 13 years growing up in Sinking Spring, a suburb of Reading, where he attended elementary and junior high school. During these early years, he developed an interest in the weather. Ted then spent his teenage years in Liverpool, New York, a suburb community of Syracuse. Here, he attended Liverpool High School from 1974-1978, where his enthusiasm for meteorology continued to grow thanks to the cold, snowy winters in central New York.

Ted pursued his profound interest at Parks College of Saint Louis University, and graduated Summa Cum Laude with a Bachelor's degree in 1982. He furthered his education by attending graduate school at Saint Louis University. Here, he worked for two semesters as a teaching assistant under Dr. James T. Moore and then for two years as a research assistant to Dr. Henry E. Fuelberg. This thesis presents the results of that research.